


# Targeting the non-ATP-binding pocket of the MAP kinase p38 $\gamma$ mediates a novel mechanism of cytotoxicity in cutaneous T-cell lymphoma (CTCL)

Xu Hannah Zhang , Chih-Hong Chen, Hongzhi Li, Jack Hsiang, Xiwei Wu, Weidong Hu, David Horne, Sangkil Nam, Jack Shively and Steven T. Rosen

Beckman Research Institute of City of Hope, Duarte, CA, USA

## Correspondence

X. H. Zhang and S. T. Rosen, Beckman Research Institute of City of Hope, Duarte, CA 91010, USA  
Tel: +1-(626)-218-9197 (X. H. Z); +1-(626)-218-7330 (S. T. R)  
E-mail: xuzhang@coh.org; srosen@coh.org

(Received 23 April 2021, revised 31 July 2021, accepted 19 August 2021, available online 15 September 2021)

doi:10.1002/1873-3468.14186

Edited by Christian Griesinger

**We describe here for the first time a lipid-binding-domain (LBD) in p38 $\gamma$  mitogen-activated protein kinase (MAPK) involved in the response of T cells to a newly identified inhibitor, CSH71. We describe how CSH71, which binds to both the LBD and the ATP-binding pocket of p38 $\gamma$ , is selectively cytotoxic to CTCL Hut78 cells but spares normal healthy peripheral blood mononuclear (PBMC) cells, and propose possible molecular mechanisms for its action. p38 $\gamma$  is a key player in CTCL development, and we expect that the ability to regulate its expression by specifically targeting the lipid-binding domain will have important clinical relevance. Our findings characterize novel mechanisms of gene regulation in T lymphoma cells and validate the use of computational screening techniques to identify inhibitors for therapeutic development.**

**Keywords:** ATP-binding pocket; computational virtual screening of chemicals; cutaneous T-cell lymphoma; cytotoxicity; lipid-binding domain; NMR spectroscopy; TCR signaling pathway; the MAP kinase p38 $\gamma$ ; TNF alpha

The human p38 mitogen-activated protein kinase (MAPK) family consists of p38 $\alpha$ , p38 $\beta$ , p38 $\gamma$ , and p38 $\delta$ . p38 $\alpha$  and p38 $\beta$  are ubiquitously expressed, but p38 $\gamma$  and p38 $\delta$  are expressed only in specific tissue types. The expression of these isoforms, and the phosphorylation of their diverse protein targets, activate many biological pathways. Sequence comparisons indicate that the p38 isoforms are about 60% similar to

one another; they are also about 40%–45% similar to three other members of the MAPK family: extracellular signal-regulated kinases (ERKs), c-jun N-terminal or stress-activated protein kinases (JNK/SAPK), and ERK/big MAP kinase 1 (BMK1) [1].

p38 kinases are directly activated by dual kinase MAP kinase kinases (MKK), in particular MKK3 and MKK6, and they play key roles in many tissues under

## Abbreviations

AA, amino acid (aa); BMK1, ERK/big MAP kinase 1; CRE, CAMP-responsive element; CSP, chemical shift perturbation; CTCL, cutaneous T-cell lymphoma; DEF, docking site for ERK, FxF; DLGH1, Drosophila disc large tumor suppressor human; EAE, experimental autoimmune encephalomyelitis; eIF-4E/MNK, eukaryotic translation initiation factor 4E/MAPK-interacting kinase; ERK, extracellular signal-regulated kinase; HD, healthy donors; HRD, His–Arg–Asp; HTVS, high-throughput virtual screening; IP, immunoprecipitation; JNK/SAPK, c-jun N-terminal or stress-activated protein kinases; LBD, lipid-binding-domain; LiVS, ligand virtual screening; MAPK, mitogen-activated protein kinase; MKI, MAPK insert; MKK, MAP kinase kinases; NCI DTP, National Cancer Institute Developmental Therapeutics Program; NFAT, nuclear factor of activated T cells; PBMC, peripheral blood mononuclear cells; PDZ domain, refers to a shared domain (80–90 aa) of three proteins PSD95, DLGH1, and ZO-1 that were first discovered; PDZ-binding motif, a motif that recognizes and interacts with PDZ domain; PSD95, postsynaptic density protein; STD, saturation transfer difference; TCR, T-cell receptor; TFs, transcription factors; TLR5, Toll-like receptor 5; UDScore, universal diversity score; ZO-1, zonula occludens-1 protein.

normal or stressful physiological conditions. Half of the substrates of p38 kinases are transcription factors (TFs), emphasizing their role in gene regulation at the transcriptional level.

A defining characteristic of each member of the p38 family is a conserved activation loop with a unique TGY (Thr180 and Tyr 182) [2,3] dual-phosphorylation motif that promotes the canonical p38 pathway. However, a T-cell-specific alternate p38 activation pathway exists *via* the phosphorylation of Y323 (p-Y323) by the tyrosine kinase ZAP70. This pathway is essential for T-cell activation [4] and differentiation [5].

p38 $\gamma$  is considered a promising therapeutic target for treating cutaneous T-cell lymphoma (CTCL) [6] because its expression, which is typically undetectable in normal T cells, is increased in CTCL [6]. p38 $\gamma$  expression has been shown to support the proliferation of diverse cancers, including colon [7], prostate [8], esophageal [9], breast [10], and liver [11]. Because p38 $\gamma$  shares an ATP-binding site with other MAP kinases, it is necessary to target its non-ATP-binding, or allosteric site, to specifically inhibit p38 $\gamma$  activity. Recently, the non-ATP-binding site of p38 $\alpha$ , also described as a lipid-binding domain, or lipid-binding-domain (LBD), has been thoroughly studied by several research groups [12–14].

A connection between the alternate activation pathway on Tyr 323 and the lipid-binding domain was first made by studies of the autophosphorylation of p38 by the MAPK insert (MKI), which undergoes significant conformational changes upon ligand binding on the LBD [12,15,16]. Several molecular mechanisms of p38 autophosphorylation at T180 have been proposed, including dimerization [16,17]. In this model, the phosphorylation of Y323 opens up a rigid region of peptides in the highly conserved HRD, followed by the auto-monophosphorylation of T180 *via* the proximal p-Y323 [17] of the other p38 monomer.

Most studies of alternative p38 activation have relied on cell-free *in vitro* assays. One study [17] hypothesized that the rigid HRD, which is highly conserved among kinases but has an unclear function [16–18], becomes pliable before autophosphorylation occurs. This possibility is supported by the fact that a single-point mutation that mimics the phosphorylation of p38 $\alpha$  at Y323 (Y323T) causes inter-lobe orientation changes. X-ray crystallography further revealed p-Y323-directed inter-lobe orientation changes as well as conformation changes on the phosphorylation lip (TGY180–182 of p38 $\alpha$ ) that result in the formation of a docking site for ERK, FxF (DEF) pocket that serves as an additional docking site for other important substrates [16,17].

p38 $\beta$  is also elevated in CTCL [6]. It is the only isoform capable of spontaneous auto-monophosphorylation of the TGY motif in HEK cells overexpressing MKK3/6 [19]. The autophosphorylation of p38 $\beta$  at Thr180 is generated by a short region composed of  $\alpha$ -G Helix and MKI, the latter of which is a major motif of the lipid-binding domain (LBD) of p38 $\alpha/\beta$  [15,20,21]. The finding is intriguing; however, the study was conducted in the HEK cell line, which lacks ZAP70 expression and has no TCR signaling pathway. Therefore, the spontaneous autophosphorylation observed must be due to allosteric effects of the classical p38 activation pathway, rather than the alternative activation pathway triggered by the phosphorylation of Y323 by ZAP70.

Direct protein–protein interactions between p38 $\gamma$  and other proteins, such as the cytoskeletal protein tyrosine phosphatase PTPN3 [22] (a negative regulator of early T-cell receptor (TCR) signal transduction and T-cell activation [23]) and nuclear factor of activated T cells 4 (NFATC4) [3], have been previously reported. We have proposed that p38 $\gamma$  interferes with TCR signaling by interacting with *Drosophila* disc large tumor suppressor human (DLGH1) and subsequently up-regulating NFATC4 *via* a unique PDZ-binding domain in p38 $\gamma$  [24]. Although we have previously reported nuclear p38 [25], its function remains elusive.

The NFAT family of proteins consists of five distinct members in humans: NFAT1 (NFATC2), NFAT2 (NFATC1), NFAT3 (NFATC4), NFAT4 (NFATC3), and NFAT5 [26]. They are TFs that modulate important functions in diverse tissues with cell-type specificity. Several studies have concluded that NFATs mediate the activation-induced cell death (AICD) of T and B cells and therefore serve as tumor suppressors in lymphoid cells [27]. NFATs modulate TNF expression through several NFAT-binding motifs in the promoter region of TNF gene [28]. NFATs also interact with ERK through their FxF motif, which docks in the ERK DEF site [29].

To better study the effect of ligand binding to the LBD/MKI of p38 on its auto-monophosphorylation activity and biological function, we devised a cell-based system using a CTCL cell line with a fully functional ZAP70 kinase capable of phosphorylating either Y323 (in p38 $\alpha/\beta$ ) or Y326 (in p38 $\gamma$ ) and in which TCR signaling is intensively activated. We confirm the presence in p38 $\gamma$  of a lipid-binding domain similar to that in p38 $\alpha$  and study the effect of ligand binding to this region. Finally, we conducted virtual ligand screening of 270 000 proteins to identify a candidate molecule that is selectively cytotoxic to CTCL cells.

Our study reveals the molecular mechanism of the conformational change that p38 undergoes in response to drugs targeting its lipid-binding domain, that is, the opening of the DEF pocket to accommodate substrates such as the TFs that modulate TCR signaling. It also suggests pathways of novel drug development for the treatment of CTCL.

## Experimental procedures

### NMR titration and chemical shift perturbation methods (2D NMR) to uncover the LBS on p38 $\gamma$

<sup>2</sup>D; Ile $\delta$ 1-[<sup>13</sup>CH<sub>3</sub>]; Leu, Val-[<sup>13</sup>CH<sub>3</sub>, <sup>12</sup>CD<sub>3</sub>]-labeled p38 $\gamma$  sample was prepared, and the NMR spectra were collected and analyzed as described [6]. In the complex sample, 100  $\mu$ M p38 $\gamma$  was added stepwise with  $\beta$ -OG or CSH71 to a molar ratio of 1 : 10. NMR chemical shift perturbation (CSP)s were calculated as.

$$CSP = \sqrt{\Delta\delta_H^2 + (0.154 \cdot \Delta\delta_N)^2 + (0.341 \cdot \Delta\delta_C)^2}$$

where  $\Delta\delta_H$ ,  $\Delta\delta_N$ , and  $\Delta\delta_C$  are the chemical shift differences between the free and bound states in the proton, nitrogen, and carbon dimensions, respectively.

### CSP normalization method

The CSP for each compound was normalized separately. The values in each dataset (different compounds) were between 0 and 1. CSPs were calculated and further normalized using the min-max method using the following equation: normalized CSP = (CSP - CSPmin)/(CSPmax - CSPmin); where CSPmax and CSPmin are the largest and smallest CSPs in each titration of the compound.

### Virtual ligand screening targeting the LBD

The LiVS pipeline was performed as described previously [30] using Glide software (Schrödinger). Briefly, the Glide high-throughput virtual screening (HTVS) mode, which is fast but less accurate, was first implemented to dock the entire NCI DTP library (270 000 compounds) onto the LBD of p38 $\gamma$ . The 10 000 top-ranked compounds were further docked and scored using Glide standard precision (SP) mode. Next, the 1000 top-ranked compounds from SP docking were redocked and rescored using the Glide extra precision (XP) mode, and were further analyzed, filtered, and narrowed down to 100 compounds using Lipinski's rule of five [31] for drug-likeness, high-throughput screen frequent hitters (PAINS) [32], and protein

reactive chemicals such as oxidizers or alkylators (ALARM) [33]. Molecular diversity was maximized by using UDScore (Universal Diversity Score), our in-house-developed compound library diversity score to measure library diversity, a universal score independent of library size.

### Cell culture and screening NCI compounds to determine cytotoxicity in Hut78

Hut78 cells cultured as previously described [6], were used to validate selected compounds. Eighty candidate compounds were obtained from the NCI DTP Open Chemical Repository. To determine the cytotoxic effect of each compound on cell viability in Hut78 cells, CellTiter-Glo assays were used (Promega, Madison, WI, USA). We seeded 7000 cells/well when using a 96-well plate and cells were collected at 2 time points, 48 and 96h treatments, respectively. IC<sub>50</sub> values were determined using CalcuSyn software (Biosoft, Cambridge, UK), as described previously [6]. Each experiment was performed in triplicate.

### Kinase assay with p38 isoforms in vitro

To characterize the selected small molecules that inhibited p38 $\gamma$ , we performed kinase assays in vitro using an ADP-Glo kit (Promega), as described previously [6]. In detail, we followed the protocol according to the manufacture production. the active kinase forms of p38 isoforms ( $\alpha$ ,  $\beta$ ,  $\gamma$ , and  $\delta$ ) were obtained from SignalChem and incubated with increasing doses of selected small molecules. A synthetic peptide substrate (IPTTPITTTYFFFKKK) was added to the mixture at a final concentration of 0.2  $\mu$ g $\cdot$  $\mu$ L<sup>-1</sup>, followed by 10  $\mu$ M ATP. The luminescent ADP-Glo kinase assay measures ADP produced from ATP consumption in the reaction. Staurosporine was used as a positive control. Luminescence was monitored at an integration time of 0.5 s using an automated BMG PHERAstar plate reader (BMG Labtech, Cary, NC, USA). Each experiment was performed in triplicate.

### NMR and competition saturation transfer difference experiment

Inactive p38 $\gamma$  protein was expressed in *E. coli* as described previously [6]. The compounds identified using LiVS were prepared as stock solutions in DMSO-d<sub>6</sub> and stored at -20 °C. Stock solution concentrations were determined using NMR with a known concentration of the reference compound sodium trimethylsilylpropanesulfonate (DSS). The buffer for

NMR experiments was composed of 15 mM Tris-d<sub>11</sub> dissolved in D<sub>2</sub>O, TCEP 1 mM, MgCl<sub>2</sub> 2 mM, and TSP-d<sub>4</sub> 50  $\mu$ M; buffer pH was 7.0. NMR saturation transfer difference (STD) [19] experiments were carried out at 25 °C on a 700 MHz Ascend magnet (Bruker) equipped with a 5-mm triple resonance cryogenic probe (spectral width 14 ppm, with 32k data points). The saturation frequency was set at  $-0.2$  ppm, and the reference experiment frequency was set at  $-30$  ppm. The 50 ms gauss pulse saturation train was 3.8 s long with field strength of 86 Hz. The T<sub>2</sub> filter spin-lock was 80 ms long with field strength of 4960 Hz. The total number of scans was 5120, and the saturation and reference experiment were acquired in an interleaved manner using Bruker stddiffgp19.3 pulse sequence. The data were analyzed using Bruker TopSpin 3.1 software. The STD was calculated using  $(I_{\text{ref}} - I_{\text{sat}})/I_{\text{ref}}$ , where the  $I_{\text{ref}}$  and  $I_{\text{sat}}$  are the peak intensity in reference and saturated spectrum, respectively. The STD error was estimated from the noise intensity of the spectrum in the range between 9.5 and 11 ppm. The sample prepared for STD measurement of CSH71 was composed of 1  $\mu$ M p38 $\gamma$ , 50  $\mu$ M CSH71, 2% DMSO-d<sub>6</sub>. For the competition STD study, an additional 100  $\mu$ M ATP was added to the sample. We also noticed that there were some residual STD values from free CSH71 under the conditions of the STD experiments used for the protein ligand complex. We obtained our final reported STD values for CSH71 in complex with protein by subtraction of the residual STD values of the free CSH71 sample obtained under the same conditions.

### Microarray analysis and RNA sequencing analysis

The Affymetrix GeneChip Human Gene 1.0-ST array (Affymetrix, Santa Clara, CA, USA) was used to define gene expression profiles from the samples. Synthesis and labeling of cDNA targets, hybridization, and scanning of GeneChips were carried out by the Integrative Genomics Core Facility at City of Hope. Briefly, cRNA was generated according to the manufacturer's protocol using Affymetrix's GeneChip Whole Transcript Sense Target Labeling Assay Hybridization cocktails containing 5.5  $\mu$ g of fragmented, end-labeled cDNA were prepared and applied to GeneChip Human Gene 1.0 ST arrays. Hybridization was performed for 16 h, and the arrays were washed and stained with a GeneChip Fluidics Station 450 using FS450\_0007 script. Arrays were scanned at 5  $\mu$ m resolution using Affymetrix GCS 3000 7G.

Raw intensity measurements of all probe sets were background-corrected, normalized, and converted into

expression measurements using Affymetrix's Expression Console v1.1.1. The Bioconductor "ArrayTools" package was then used to identify the genes differentially expressed between the treated and untreated samples. Significant genes were selected with a cutoff of adjusted  $P < 0.05$  and fold change of 2. The DAVID functional annotation tool (<https://david.ncifcrf.gov/content.jsp?file=citation.htm>) was then used to identify modulated KEGG signaling pathways.

## Immunoprecipitation and western blot analysis

### Immunoprecipitation with beads

Antibodies were added to protein lysates at recommended dilutions and incubated at 4 °C overnight with rotation. Magnetic beads (Dynabeads protein G, #10004D Life Technologies, Waltham, MA, USA) were washed with lysis buffer then added to the lysate-antibody mix. The bead-antibody-lysate mixtures were left to incubate at room temperature for 60 min with rotation. Beads were washed with cold PBST 4 times and subsequently resuspended in loading buffer and boiled for 5 min. The samples in loading buffer were separated from beads and moved to a fresh clean tube. Western blot (WB) analysis was performed as described previously [6]. Primary antibodies purchased from Cell Signaling Technology (Danvers, MA, USA) were used at the following dilutions: p38 $\alpha$  (#9218, 1 : 1000), p38 $\beta$  (#2339, 1 : 1000), p38 $\delta$  (#2308, 1 : 1000), p38 $\gamma$  (#2307, 1 : 1000), p-p38 T180/Y182 (#4511, 1 : 1000), NFACT C1 (#8032, 1 : 1000), Lamin A/C (#4777, 1 : 5000), and GAPDH (#2118, 1 : 5000). Primary anti-SAPK3 (ab205926) was purchased from abcam (Cambridge, MA, USA) and used at 1 : 1000 dilution. Primary p-p38 Y323 antibody (#12322-1) was purchased from Signalway Antibody and used at 1  $\mu$ g·mL<sup>-1</sup>. Primary anti-PTPN3 (#NBP2-78797, 1 : 1000) was purchased from Novus, Goat anti-rabbit HRP-linked antibody (GE #NA934, 1 : 2500) was used as secondary antibody.

### Nuclear and cytosolic protein extraction

Nuclear and cytosolic proteins were extracted from cells using the NE-PER Nuclear and Cytoplasmic Extraction Kit (Thermo Fisher 78833, Waltham, MA, USA). Briefly, fresh cells were pelleted and washed with cold 1x PBS, followed by resuspension in CER I buffer by vortexing. After a 10-min incubation on ice, CER II buffer was added to the mixture, which was then pelleted *via* centrifugation. After centrifugation, the supernatant (containing cytoplasmic proteins) and



pellet (containing nuclei) were separated by pipetting. Similarly, nuclear proteins were extracted from pellets by adding NER buffer and performing vigorous vortexing and subsequent centrifugation. Supernatants were collected as nuclear protein lysates. Protein lysates were quantified using the BCA assay, mixed with loading dye containing  $\beta$ -mercaptoethanol, and boiled for 5 min on a hotplate.

### Confocal fluorescence microscopy

Materials and methods of Immunofluorescence staining and microscopy with Hut 78 cells followed instructions as previously described [34]. For DLGH1 staining, we used antibody against Goat-DLGH1, (Invitrogen, Waltham, MA, USA, Cat. #PA5-18790) and detected using Texas red conjugated donkey anti-goat IgG (red) (ThermoFisher, Cat. #PA1-28662); for alternative p38 activation detection, we stained cells with Rabbit antibody against phosphor-p38 at Y323 (ThermoFisher, Cat. # PA5-40258), Donkey anti-Rabbit 650 Dylight (abcam, ab96894) was then used as secondary antibody. For IL17RA staining, we chose mouse antibody IL17RA (R & D, Minneapolis, MN, USA, MAB4481) as primary antibody, and FITC conjugated Goat anti-mouse as secondary antibody. Stained cells were washed and mounted with the mounting medium Vectashield (Vector Laboratories, Burlingame, CA, USA). The cells were counterstained with 4-6-diamidino-2-phenylindole (DAPI) (blue) and analyzed by fluorescence microscopy with a confocal scanning microscope (Zeiss LSM 510 META or Zeiss LSM 700, Oberkochen, Germany) with a  $\times 63$  or  $\times 100$  objective. Confocal laser scanning microscopy was performed at Light Microscopy Shared Resource Facility of City of Hope.

### Statistical analysis

Data are expressed as the mean  $\pm$  SD. The statistical significance of differences was analyzed using Student's *t*-test, where  $P < 0.05$  was considered significant.

## Results

### Conservation of the lipid-binding domain among p38 isoforms

It is well known that p38 $\alpha$  harbors a lipid-binding domain (LBD) that exerts allosteric functions on its ATP-binding pocket [12,17]. We compared amino acid sequences in the lipid-binding domain among all four p38 isoforms and found the site to be highly conserved

in the p38 family (Fig. 1A). The sequence and structural similarities between the p38 $\gamma$  and p38 $\alpha$  isoforms suggest that p38 $\gamma$  may also contain a lipid-binding domain.

The lipid-binding domain in p38 $\alpha$  was so named because the first small molecule discovered to bind to this site was the lipid-like detergent n-octyl-beta-glucopyranoside ( $\beta$ -OG, Fig. 1B,C). We confirmed that  $\beta$ -OG was among 17 small molecules (Fig. 1D) that exclusively bind the LBD of p38 $\alpha$  by comparing 253 publicly available X-ray crystallographic structures of p38 $\alpha$ -compounds deposited in the RCSB Protein Data Bank (PDB). The chemical structure of  $\beta$ -OG (Fig. 1C, top) and its 2D interaction with p38 $\alpha$  (Fig. 1C, bottom) depict the hydrophobic tail of the chemical surrounded by hydrophobic residues of p38 $\alpha$ . In addition to the 17 molecules that bind only the LBD, six molecules—GG5 (PDB: 3hvc), p41 (PDB: 3c5u), D13 (PDB: 1ian), 279 (PDB: 2rg6), 80T (PDB: 5n65), and 6RG (PDB: 4dlj)—bind to two sites on p38 $\alpha$ : the ATP-binding site and the lipid-binding domain (Fig. 1D–E). The biological functions of these two site-binding molecules are still unclear [11,12,13,14,35,36,37,38].

p38 $\alpha$  also contains a Docking site for ERK *via* motif of ERK – FXFP, or DEF site near the LBD [16]. We hypothesized that ligand binding to the LBD allosterically triggers the opening of the nearby DEF pocket to accommodate the binding of diverse substrates and render a spectrum of biological effects. To test this hypothesis, we showed that molecules that bind LBD allosterically alter the structure of the ATP-binding site, as evidenced by the crystal structures of p38 $\alpha$  in complex with  $\beta$ -OG (Fig. 1F, PDB: 2npq).

### Demonstration of an LBD on p38 $\gamma$ using NMR

To determine whether p38 $\gamma$  also has an LBD, we used two-dimensional NMR CSP, or chemical shift perturbation, to investigate the interaction between  $\beta$ -OG and p38 $\gamma$ . Two-dimensional NMR spectroscopy allows the study of site-specific interactions with mM binding affinities under near-physiological conditions, and it reveals structural information that may otherwise be difficult to obtain by X-ray diffraction. It can rapidly identify binding sites on target proteins, as well as conformational changes triggered by compound binding.

We monitored the chemical shift perturbation of p38 $\gamma$  in both  $^1\text{H}$ - $^{15}\text{N}$  HSQC and  $^1\text{H}$ - $^{13}\text{C}$  HMQC spectra alone, and in the presence of  $\beta$ -OG (Fig. S1A,B). We found that residues with significant NMR CSPs (magenta) were localized primarily around the MKI motif (CSP cutoff for amides at 0.02 ppm (Fig. S1C)

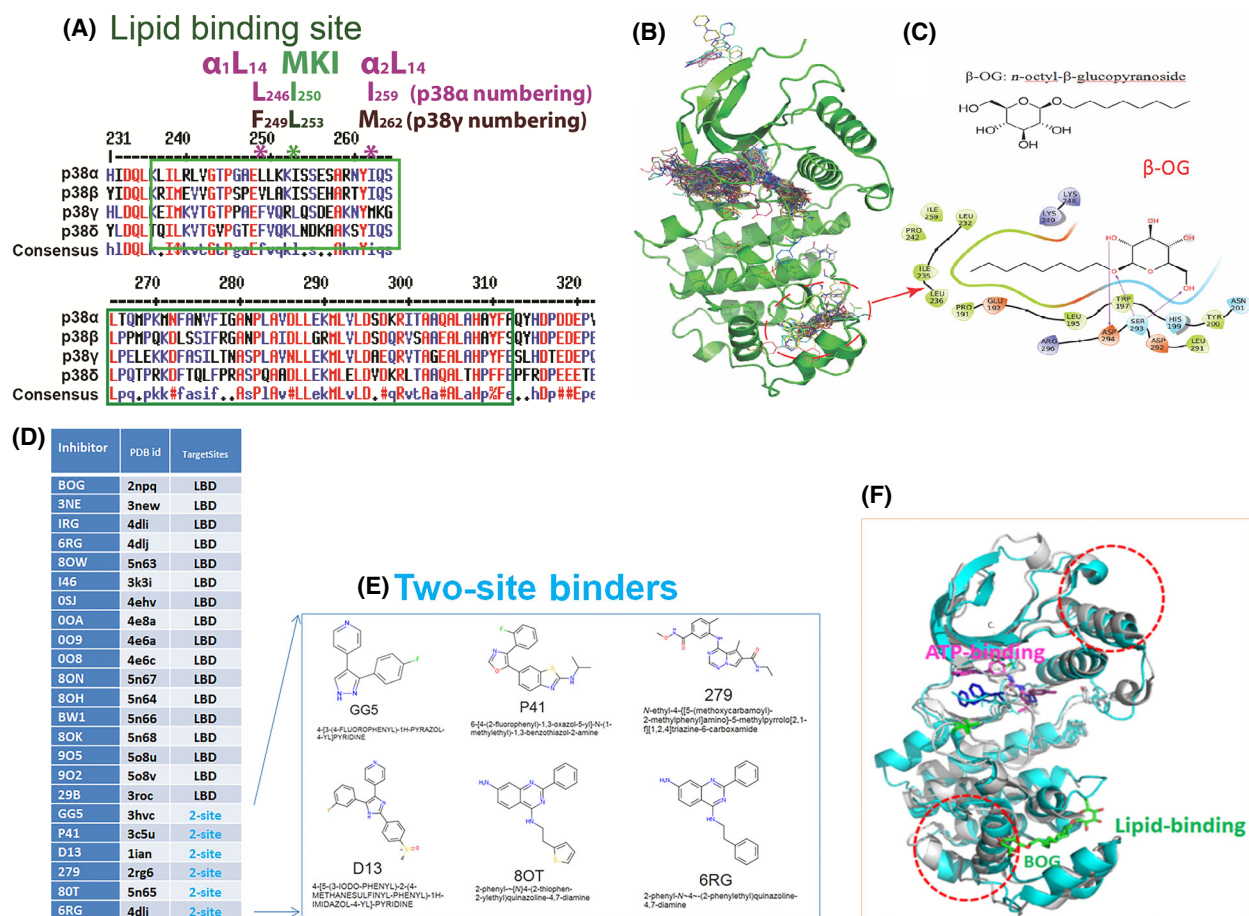


**Fig. 1.** Lessons we learnt from p38 $\alpha$  on LBD. (A) Consensus amino acids sequences alignment diagram in the lipid-binding domain among four p38 isoforms by clustalW2. MARP insert harbors LBD which is between two  $\alpha_{1L_{14}}$  helices,  $\alpha_{1L_{14}}$  and  $\alpha_{2L_{14}}$ . L246 and I259 are two conserved residues of p38 $\alpha$  in two L14 loops that indicated in \*. Likewise, the counterparts of above two residues in p38  $\gamma$  are F249 and M262 that are conserved. (B) structures of ligands bound to p38 $\alpha$  from 253 PDB entries that have X-ray Crystallography structures. Most of the ligands are single-site binders, either on the ATP-binding site or the lipid-binding site, while some ligands bound to two sites simultaneously. Circled is the area  $\beta$ -OG bound at the lipid-binding pocket. (C) Chemical structure of  $\beta$ -OG (n-octyl- $\beta$ -glucopyranoside, top) and 2-dimensional (2D) interaction diagram of  $\beta$ -OG in complex with p38 $\alpha$ . The hydrophobic tail of  $\beta$ -OG is surrounded by hydrophobic amino acids of p38 $\alpha$  (bottom). (D) 17 small ligands of the p38 $\alpha$  solely target lipid-binding domain (LBD) and 6 small molecules targets both LBD and ATP binding pocket (data summarized from X-ray crystallography). The column of TargetSites shows the number of sites for a ligand; 2-site (teal color) means that the inhibitor binds at both the lipid-binding site and ATP-binding site simultaneously, and LBD indicates the inhibitor can only bind LBS site of p38 $\alpha$ . Only one PDB id is listed for each small molecule. (E) Two site binders of p38 $\alpha$  with X-ray crystallography structure consist of 6 molecules: GG5 (PBD: 3hvc); p41 (PBD: 3c5u); D13 (PBD: 1ian); 279 (PBD: 2rg6); 80T (PBD: 5n65); and 6RG (PBD: 4dlj) are ligands for two sites, that is, the ATP binding and the lipid-binding of p38 $\alpha$ . (F)  $\beta$ -OG lipid binding of p38 $\alpha$  may cause allosteric effects on ATP binding. We superimposed two public PDB datasets from RCSB, the DFG-out conformation of p38 $\alpha$  alone (PDB 2ba<sub>j</sub>) is displayed as cyan cartoons; and the inactive p38 $\alpha$  bound  $\beta$ -OG as grey cartoons (PDB 3gc<sub>v</sub>). When  $\beta$ -OG bound, the structure is changed significantly near both the lipid-binding and ATP-binding sites (depicted as dotted red circles), which suggests that the binding of  $\beta$ -OG at the lipid-binding site causes conformational changes near the ATP-binding site and thereby affect its kinase activity allosterically.

and methyls at 0.03 ppm (Fig. S1D)). Figure 2A summarizes both spectra NMR CSP and indicates those residues that are greatly perturbed by  $\beta$ -OG (orange). Figure S1E shows that all our NMR CSP procedures have titrated molar ratios,  $\beta$ -OG (the variable) to p38 $\gamma$  (the constant). Ratios (p38 $\gamma$ /  $\beta$ -OG) are 1 : 0 (red, no  $\beta$ -OG as control), 1 : 2.5 (yellow), 1 : 5 (green), 1 : 7.5

(cyan), and 1 : 10 (blue). Based on these results, we generated a three-dimensional structure of  $\beta$ -OG bound to the LBD of p38 $\gamma$  (Fig. 2B) using p38 $\gamma$  crystallography structure coordinate datasets downloaded from RCSB PDB [PDB id 1cm8 [39]]. The NMR titration data indicate specific binding of  $\beta$ -OG to p38 $\gamma$  in the LBD.

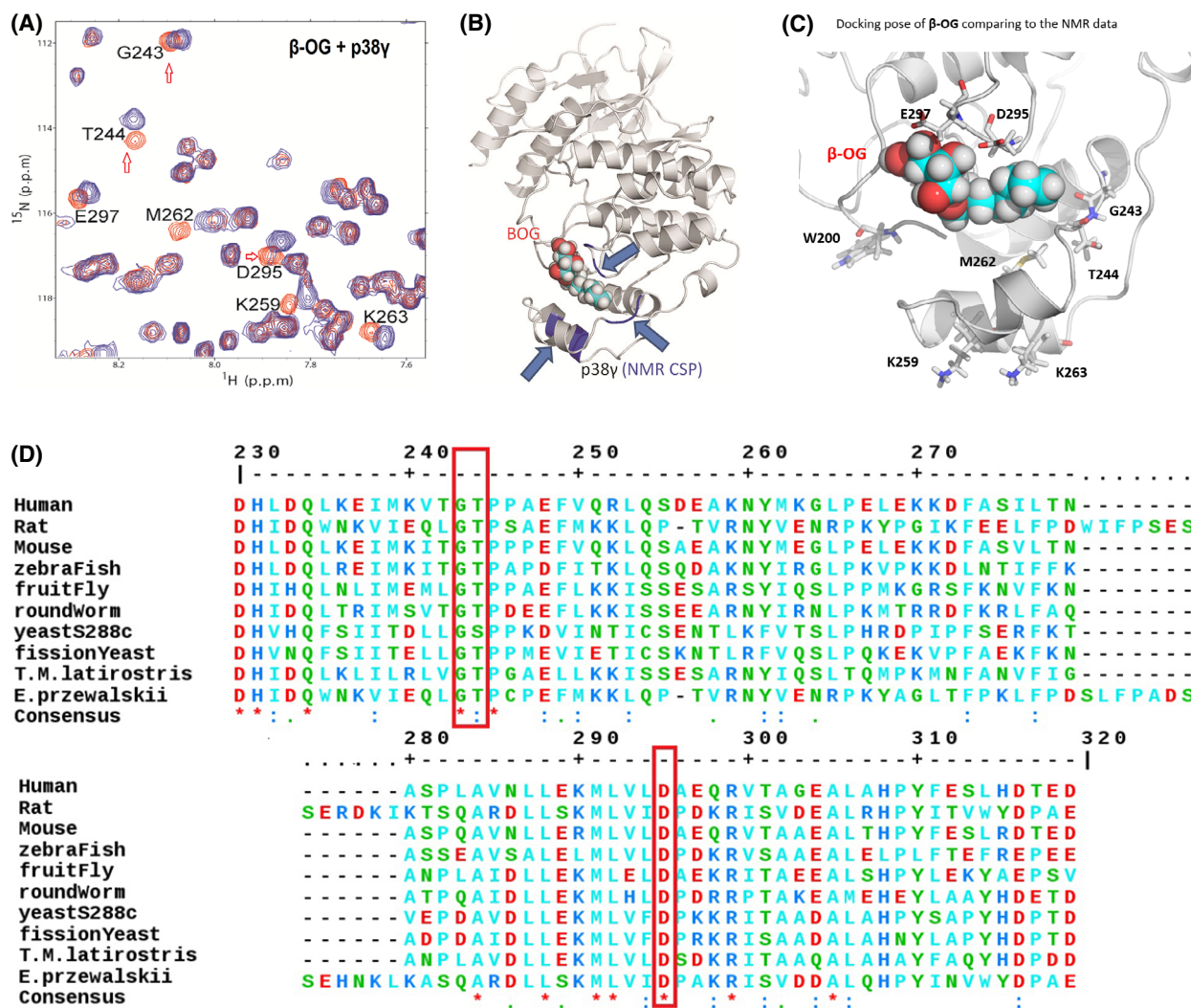


**Fig. 2.** NMR demonstrates a lipid-binding site on p38 $\gamma$  for  $\beta$ -OG. (A) 2D NMR CSP experiment locates the p38 $\gamma$  residues that significantly shifted due to addition of  $\beta$ -OG, indicated in orange. NMR CSPs data by monitoring  $^1\text{H}$ - $^{15}\text{N}$  HSQC and  $^1\text{H}$ - $^{13}\text{C}$  HMQC spectra upon the addition of  $\beta$ -OG alone and p38 $\gamma$  to  $\beta$ -OG with a molar ratio of 1 : 10. The red hollow arrows indicate three residues, G243, T244, and D295 that are conserved among species from human to yeast (See also Figure 2D, red bracket). (B) The structures of p38 $\gamma$  in complex with  $\beta$ -OG. A 3D structural model presenting where  $\beta$ -OG bound to LBD of p38 $\gamma$ , based on NMR CSP titration data. The p38 $\gamma$  crystallography structure coordinate datasets were downloaded from RCSB PDB [PDB id 1cm8 [39]]. (C)  $\beta$ -OG binds p38  $\gamma$  in the MKI region of in the lipid-binding domain and residues which greatly perturbed residues in NMR CSP assay are W200, M262, G243, D295, and E 297. K259 and K263 are consistent with that of alpha p38 which are perturbed by B-OG in Figure 1F. (D) ClustalW2 consensus alignment diagram of amino acid sequences in the lipid-binding domain of p38 $\gamma$  among indicated species.  $\beta$ -OG NMR CSP perturbed residues of human p38 $\gamma$ : G243, T244, and D295 (in red brackets) are conserved among species including yeast. Three residues E297, K259, and M262 share homology with mouse.

Our results indicate that LBD-bound  $\beta$ -OG perturbs several nearby residues, including W200, M262, G243, D295, and E297 (Fig. 2A,C). Two of these residues are among three (indicated in Fig. 2A by red arrows) that are highly conserved from yeast to humans (Fig. 2D), suggesting an important function for the LBD in p38 $\gamma$ . Taken together, our results demonstrate for the first time that p38 $\gamma$  contains an LBD for the ligand  $\beta$ -OG.

### Identification of compounds that bind p38 $\gamma$ LBD using virtual ligand screening

To identify additional compounds that bind to the LBD of p38 $\gamma$  and thus could serve as potential inhibitors of the enzyme, we implemented an in-house-developed Ligand Virtual Screening (LiVS) pipeline [30] to screen the NCI DTP library (270 000







obtained from NCI DTP for further experimental validation.

### Biological validation of CSH71 and CSH18CN using cytotoxicity measurements in CTCL cells

We treated Hut78 CTCL cells with increasing doses of each of the candidate compounds for 72 h to determine whether any were cytotoxic against CTCL. Of the 80 compounds computationally predicted to bind to the p38 $\gamma$  LBD, two—CSH18 (NSC109833) and CSH71 (NSC381863)—exhibited drastically different structures (Fig. 3B, bottom). Both were cytotoxic to Hut78 cells, with IC<sub>50</sub> = 3.4  $\mu$ M and 33 nM, respectively (Table 1). Mass spectrometry indicates that CSH71 from NCI DTP is a mix of three fractions (Fig. S2A). Here, we focused on Fraction 3 which is pure CSH71 (Fig. S2B). We also synthesized CSH71 commercially. CSH18 (NSC109833) is predicted to be an alkylator, therefore, we replaced the -Br group with -CN (CSH18CN, Fig. 3B, bottom), which we also had commercially synthesized. The purity of both commercially synthesized compounds is over 95% (data provided upon request).

Pure CSH71 showed cytotoxic effects in Hut78 cells, with IC<sub>50</sub> = 2.2  $\mu$ M at 72 h (Fig. S3A). In comparison,  $\beta$ -OG is cytotoxic to Hut78 cells at IC<sub>50</sub> = 1.76 nM. Although CSH71 and CSH18CN are each cytotoxic to Hut78 cells (Fig. 4A, 48 h; and B, 96 h, top), peripheral blood mononuclear cells (PBMC) from healthy

donors (HD)—in which p38 $\gamma$  expression is undetectable—were unaffected even at high doses.

As described above,  $\beta$ -OG binds only to the LBD of p38 $\gamma$ . To investigate the effects of molecules that bind solely to the ATP-binding site of p38 $\gamma$ , we used the multi-kinase inhibitor F7/PIK75, which we have previously shown binds to the ATP-binding site in p38 $\gamma$ . Interestingly, unlike CSH18 and CSH71, which bind two sites on p38 $\gamma$ , F7 (which targets only the ATP-binding site) and  $\beta$ -OG (which targets only the LBD), are cytotoxic to both healthy PBMC and Hut78 cells (Fig. 4A 48 h and B 96 h, bottom).

In vitro kinase activity assays in the presence of increasing concentrations of CSH71 up to 200  $\mu$ M indicate it has no effect on p38 $\gamma$  kinase activity (Fig. S3D)—further suggesting that the kinetics of two-site-binding ligands differ from those that recognize only the ATP-binding site. Further investigation on other p38 isoforms confirmed it also does not inhibit their kinase activity (Fig. S3C).

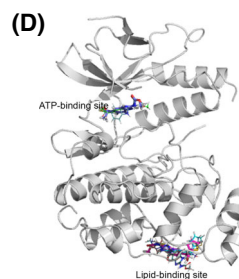
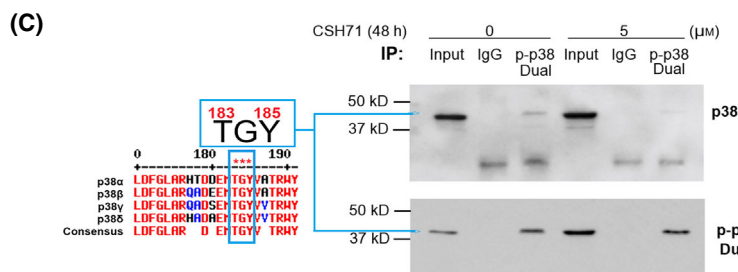
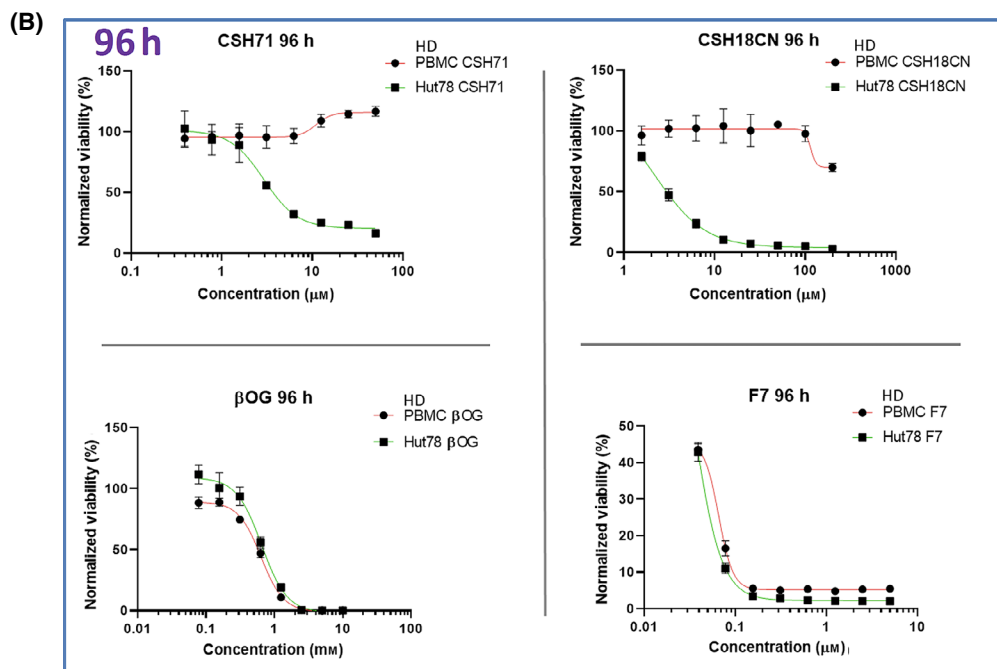
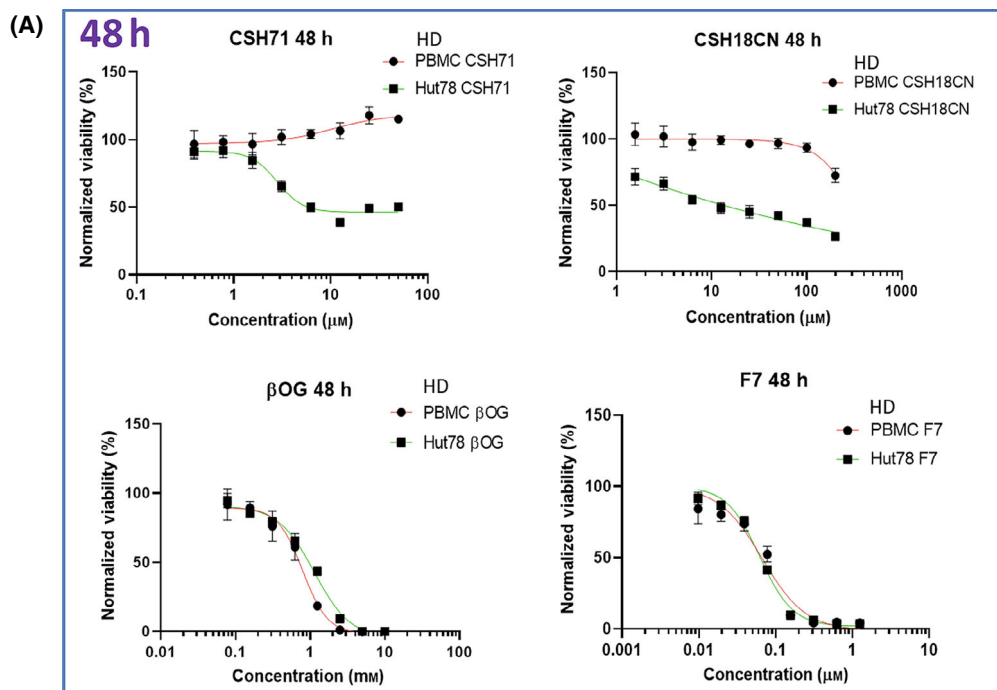
There are four isoforms of human p38, all of which contain a conserved motif (“TGY motif”) in each activation loop, regardless of its position—that is, whether it is positioned as dual phosphorylation of Thr180-G-Tyr182 (in p38  $\alpha$ ,  $\beta$ , and  $\delta$ ) or Thr183-G-Tyr185 (in p38 $\gamma$ )—as the length of polypeptides of p38 isoforms are slightly different (See Fig. 4C left). We reasoned that the antibody against dual phosphorylation p-p38 (CST # 4511) can recognize all dual phosphorylation combinations of this motif in all four p38 isoforms.

To validate the concept that p38 $\gamma$  contains a p-p38 dual phosphorylation site positioned at Thr183-G-Tyr185, we first performed an immunoprecipitation (IP) study by pulling down all dual-phosphorylated p38 with antibodies against p-p38 dual phosphorylation (CST #4511) and then detected p38 $\gamma$  among the immunoprecipitated dual-phosphorylated p38 protein using a total p38 $\gamma$  antibody (CST #2307). By comparing that with isotope IgG control (Fig. 4C right, immunoprecipitation, IP experiment), we concluded using this indirect approach (i.e. IP) that the dual

**Table 1.** IC<sub>50</sub> ( $\mu$ M) of Hematopoietic cell lines that are sensitive to CSH18 and CSH71.

	CSH18	CSH71	
Hut78	3.4	0.033	CTCL
HL60	3	0.73	AML
MOLT4	0.24	0.29	ALL
K562	0.54	0.27	CML
CCRF-CEM	0.1	0.05	AML
SR	0.11	0.27	Lymphoma
RPMI-8226	7.8	4.8	MM

**Fig. 4.** Cytotoxicity measurements of pure CSH71 and CSH18CN in CTCL cells. (A and B) Cytotoxicity assays and IC<sub>50</sub>s determination of newly synthesized compounds which are considered as two site binders CSH71 and CSH18CN Hut78 CTCL cells treated with increasing doses, respectively, for 48 h (A.) and 96 h. (B). F7 and  $\beta$ -OG, served as one-site binder, ATP binding and lipid-binding of p38 $\gamma$ , respectively. PBMC from healthy donors (HD) used as a control as its p38 $\gamma$  level is at undetected level. Rest of text we focus on CSH71 for further analysis of its biological activity due to its interaction with the p38 $\gamma$  LBS. (C) Enrichment of dual-phosphorylated p38 by Immunoprecipitation (IP). Sequence of p38 isoforms that all contain TGY motif dual activation site T<sub>180/183</sub> GY<sub>182/185</sub> (for p38 $\gamma$  the motif is T183-G-Y185, all other isoforms are T180 and Y182, Left). Right: IP results, first pulling down with dual-p-p38 of p38 antibody, then detect with p38 $\gamma$  and dual-p p38 antibody, respectively, in cytosol of Hut78 cells both untreated (0  $\mu$ M) and CSH71-treated (5  $\mu$ M). The blue arrow points to p38 $\gamma$  that contains dual phosphorylation p-p38 at T183-G-Y185. (D) CSH71 has only two predicted binding sites of p38 $\gamma$  by all around docking pose commutating analysis; and the MaxGScores of ATP-binding and lipid-binding, are -6.82, and -6.18 kcal·mol<sup>-1</sup>, respectively, which also indicates the binding affinity of CSH71 in LBD is much weaker than that of  $\beta$ -OG with a MaxGScore of -8.9 kcal·mol<sup>-1</sup>.



phosphorylation-enriched p38 contains p38 $\gamma$ , in which the dual phosphorylation sites are positioned at Thr183 and Tyr185 based the above background information.

Computational analysis of the interaction of CSH71 with p38 $\gamma$  indicates that it binds to the ATP-binding site as well as the LBD, with MaxGScores of  $-6.82$ , and  $-6.18$  kcal $\cdot$ mol $^{-1}$ , respectively. Therefore, the binding affinity of CSH71 to p38 $\gamma$  is much weaker than that of  $\beta$ -OG to the LBD (MaxGScore =  $-8.9$  kcal $\cdot$ mol $^{-1}$ , Fig. 4D).

For decades, kinase inhibitor drug development has focused on blocking the molecule's ATP-binding site. Our data deliver an important novel message that simultaneously targeting both the lipid-binding domain and ATP-binding site may be a more effective and specific approach.

### Demonstration of CSH71 binding to p38 $\gamma$ by 1D NMR STD

Saturation transfer difference is an NMR method based on the phenomenon that proton saturation on a protein can be transferred to an interacting ligand. The STD monitors the ligand proton peak intensity difference in the presence and absence of saturation on protein protons. STD is suitable to detect interaction with ligands with dissociation constants  $K_D$  ranging from  $10^{-3}$  to  $10^{-8}$  M, and, because the region of the ligand that interacts most closely with the target protein shows the largest peak intensity changes, it is also a useful way to identify and map ligand binding epitopes. The extent of variation of STD values within the ligand is used to determine the specificity of the interaction [40].

To further understand the nature of CSH71 binding to p38 $\gamma$ , we performed STD NMR on the CSH71-p38 $\gamma$  complex alone and in the presence of increasing concentrations of ATP (Fig. S4A,B) to determine whether ATP competes with CSH71 for binding to the p38 $\gamma$  ATP-binding pocket (Fig. 4D). STD values varied from approximately 56% to 59% among the aromatic peaks of CSH71 in the absence or presence of ATP, respectively. These observations suggest that the interaction is not due to random binding [40,41] of CSH71 with p38 $\gamma$ . The docking pose at the ATP-binding site closely resembles the NMR STD result—with the five-ring group inside the pocket, while the—COOCH<sub>3</sub> tail of CSH71 remains outside the ATP pocket (Fig. S4A, top and Fig. S4C, left). CSH71 binding to the LBD pocket is more flexible, however (Fig. S4A, bottom and Fig. S4C, right). These results are consistent with a model in which CSH71 binds first to the ATP-binding

site, as predicted both computationally and by our NMR 1D result (in the absence of ATP).

To mimic conditions in living cells, we performed ATP replacement experiments using STD NMR on the CSH71-p38 $\gamma$  complex in the presence of increasing concentrations of ATP. Although the high-affinity binding of ATP displaces CSH71 from the ATP-binding site, its addition does not reverse the changes of aromatic peaks of CSH71 on p38 $\gamma$  observed as the stable STD value (Fig. S4B), again indicating that CSH71 binds more than one site on p38 $\gamma$ .

### Demonstration of CSH71 binding to p38 $\gamma$ at LBD by 2D NMR CSP

To more precisely locate the p38 $\gamma$  residues bound by CSH71, we performed 2D NMR chemical shift perturbations (CSP) titration experiments using CSH71. In  $^1\text{H}$ - $^{15}\text{N}$  correlation spectra (amides), CSH71 resulted in significant CSPs on the residues V33, G39, A40, V41, Y326 (colored red, CSP > 0.02 ppm); disappeared residues F111 and G117 are shown as magenta sticks (CSP > 0.02 ppm; Fig. S5A,C). The disappearance of certain residues suggests tight binding of CSH71 to p38 $\gamma$ .

To compare independent NMR CSP results between two different chemicals—CSH71 (which binds to two sites on p38 $\gamma$ , blue round dots) and  $\beta$ -OG (which binds only to the LBD, green triangles)—we normalized the  $^1\text{H}$ - $^{15}\text{N}$  NMR CSP results for CSH71, and overlaid the results with those of  $\beta$ -OG (Fig. 5A). The shifted residues in the ATP-binding region induced by CSH71, with a cutoff value of 0.5 of normalized CSP value, are V33, G39, A40, V41, and K69. The shifted residues in the LBD induced by CSH71 are T244, I276, and E312 (Fig. 5A, blue round dot).  $\beta$ -OG, in contrast, shifts residues solely in the region of the LBD: G264, T244, M262, D295, I259, and D294 (Fig. 5A, green triangles).

When we adjusted the basal line of normalized CSP to 0.18 ( $^1\text{H}$ - $^{15}\text{N}$  NMR), based on that of  $\beta$ -OG, we can see more residues in the LBD shifted by CSH71—L198; M219; M262, and V300—as well as others near the alternative phosphorylation site—Y326 (amides shifted residues) and V323 and V333 (methyl shifted residues). In summary, both CSH71 and  $\beta$ -OG shift residues G243, E248, L253, K263, L294, D295, A296, and R299, which confirms experimentally that CSH71 binds the LBD of p38 $\gamma$  (Fig. 5A).

Additionally, we also observed another motif Helix L16 in the C-terminal that is greatly shifted in both  $^1\text{H}$ - $^{15}\text{N}$  and  $^1\text{H}$ - $^{13}\text{C}$  spectra (Fig. 5A,B). L16 loops covers residues L337, V343, and L357 (the methyl shifted residues), their sequence is at C-terminal but

3D structure is at N-lobe. In Fig. 5E, we showed that red Helix L16 flips back to the p38 $\gamma$  at N-lobe, suggesting any shifts in the region affect the ATP-binding pocket *via* allosteric effects.

We also observed HRD and the DFG site being shifted. In  $^1\text{H}$ - $^{13}\text{C}$  spectra (methyls), L58 and I149 are shifted, and the disappeared residues are M109CE, L170CD1, and L174CD1 (Fig. 55B, D), in the region depicted in the overlaid NMR CSP spectra as covering the HRG and the DFG site (D171-F172-G173) (Fig. 5 B). Our NMR CSP (methyl group) data support this notion and indicate that the HRD motif of p38 $\gamma$  and its adjacent residues I149, L154, L159, V161, I169, and L170 in  $^1\text{H}$ - $^{13}\text{C}$  (Methyl, Fig. 5B, in the pink bracket) were highly perturbed by CSH71.  $^1\text{H}$ - $^{15}\text{N}$  spectra residues D164- A178 that covers  $\beta 8$  and DFG motif also were shifted (Fig. 5A, yellow circle). Together with the computational 2D interaction diagram (Fig. 5C), this result suggests that the ligand-LBD binding results in conformational changes in HRD by CSH71 (Fig. 5D).

In addition, L89 of  $\beta$ -sheet 4 of N-lobe p38 $\gamma$  (Fig. 5E) is also greatly shifted. It suggests the N-lobe of the p38 $\gamma$ -CSH71 complex experienced significant structural changes that can only be deciphered by X-ray crystallography, which is out of the scope of this study. It is worth noting that residue Y326 of p38 $\gamma$ —the counterpart of the alternative phosphorylation site Y323 in the p38 $\alpha$  and  $\beta$  isoforms—is significantly shifted by CSH71 (Fig. 5A, red circle). The biological significance of this shift is discussed in the following sections.

### DEF site formation of p38 $\gamma$

The DEF site of p38 is a functional domain that can accommodate various ligands, each of which triggers a specific biological outcome [3,16,42,43]. Portions of the DEF are conserved across all four p38 isoforms (Fig. 6 A, top). These segments also contain key residues of the lipid-binding domain, as the MKI is one of its critical motifs. The X-ray crystallographic structure of p38 $\alpha$  indicates that W197 serves as an important anchor in the lipid-binding pocket for lipid-like ligands [13,35,37,38]. Our NMR 2D CSP results suggest that W200 of p38 $\gamma$  (the counterpart of W197 in p38 $\alpha$ ) anchors  $\beta$ -OG on the top in the lipid-binding domain with  $\alpha 1\text{L}14$  and  $\alpha 2\text{L}14$  helices at the bottom (Fig. 2C).

Further analysis of the NMR CSP data on the DEF pocket of p38 $\gamma$  indicated that residues I197 and L198 (the counterpart of L195 of p38 $\alpha$ ) were greatly shifted and that H231 (the counterpart of H228 of p38 $\alpha$ ) could be very dynamic and pliable. Residue H231 was not observable from a 2D spectrum of the apo form of p38 $\gamma$  that assumed even greater perturbation by

CSH71. Residues L220, T221, and T224, which surround H231, are significantly shifted, as well as residues T244, A258, M262, K263, G264, and L265 in the MKI region (Fig. 5A,B and 2A,D). Three of these residues are conserved among species: H231, G243, and T244 (Fig. 2C,D indicated by \*). Our data suggest that the DEF interaction pocket may open due to shifted segments HRD-DFG, inter-lobe (Y326) and  $\beta$ -sheet 4 (L89) in the N-lobe, which lead to significant structural changes on inter-lobe of p38 $\gamma$  upon CSH71 binding. In theory, this would further promote the accommodation of TFs such as NFATs [29].

Residues predicted to be involved in the DEF pocket of p38 $\gamma$  are L198, H231 and A258, M262, and L265 (Fig. 2C; 5A, yellow circle; Fig. 5B, pink bracket), most of which are perturbed or disappeared in our CSP NMR assay in Fig. 5A,B. Figure 6E (bottom right) summarizes our data indicating that a DEF pocket is likely formed in p38 $\gamma$  upon LBD binding. This pocket then is able to accommodate NFAT *via* its FXF motif in the REL domain.

### Alternative activation of p38 co-related to TNF $\alpha$ mRNA expression upon treatment of CSH71 at lower dosage

p38 isoforms harbor both a phosphorylation lip (the dual phosphorylation site TGY [T183–Y185 in p38 $\gamma$ ]) and a C-terminal tail segment with the alternative phosphorylation site Y323 as well as the L16 loop and Helix L16. p38 $\gamma$  is unique in its alternative activation site at Y326, and the PDZ-binding motif in the C-terminal domain (RxSxETPL, Fig. 6A, bottom right). The PDZ-binding motif modulates NFAT transcriptional activation [44] through an interaction with the PDZ domain of DLGH1, which is a p38 $\gamma$  kinase substrate (*via* its ATP site). DLGH1 activation is known to drive the TCR pathway to NFAT rather than NF $\kappa$ B [44].

To determine the efficacy of alternative p38 activation in Hut78 cells following treatment with CSH71, we monitored by western Blot the protein levels of p38 isoforms and p38 dual (p-p38 TGY) and alternative phosphorylation forms (p-p38 at Y323) of cells treated with increasing dosages of CSH71. Our data showed increasing phosphorylation of p38 at Y323 in response to increasing doses of CSH71 up to 500nM and a decrease in dual p38 phosphorylation at this dosage after 24 h of exposure (Fig. 6B).

Based our cytotoxicity studies of CSH71 in Hut78 cells ( $\text{IC}_{50} \sim 2 \mu\text{M}$ ), we chose 500 nM as a low dose to study the effect on nuclear NFATs because CSH71 induces alternative p38 activation at concentrations



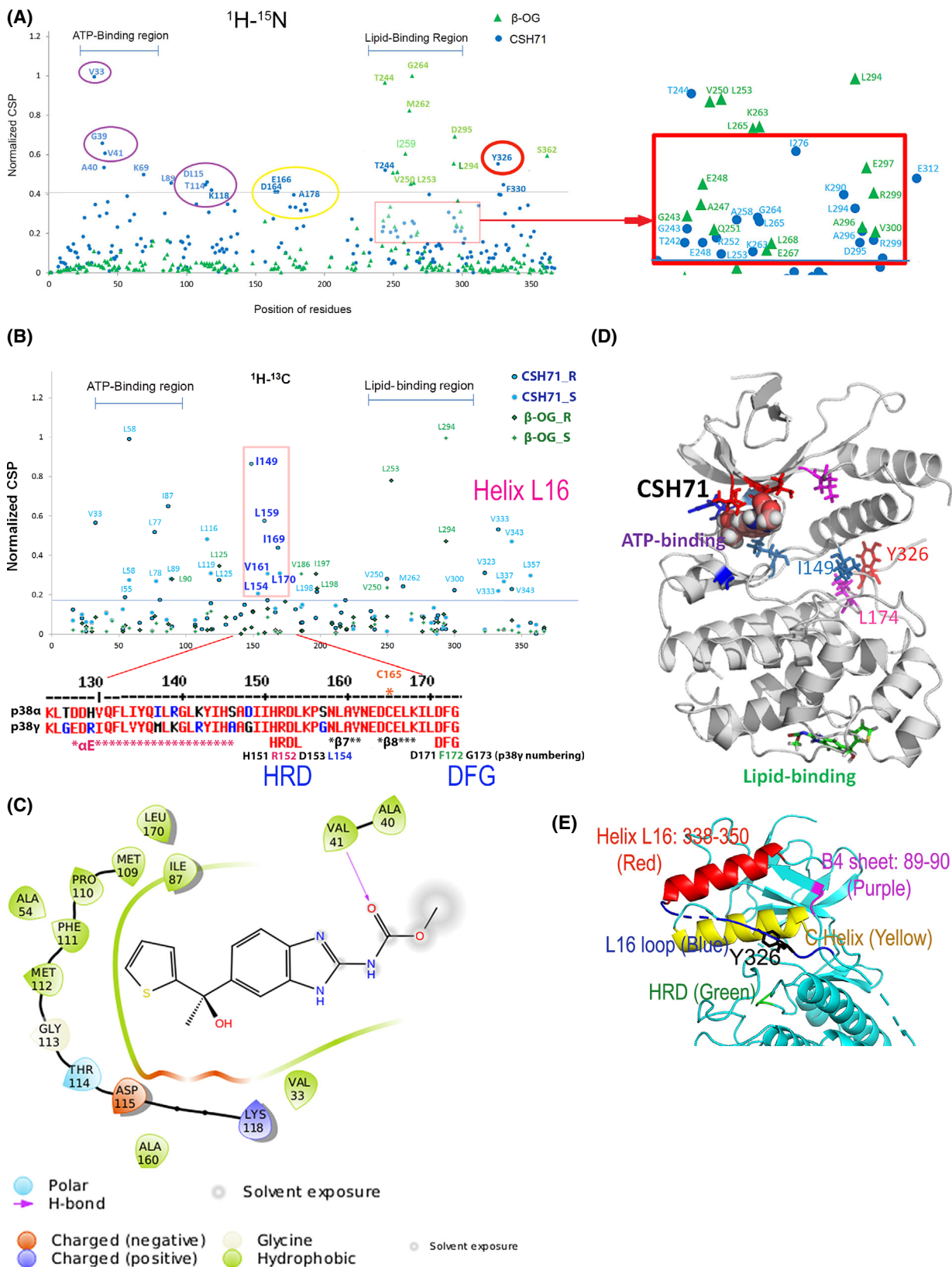


**Fig. 5.** Compound CSH71 binds to two sites on p38 $\gamma$  in cell-free based system. (A) NMR CSP  $^1\text{H}$ - $^{15}\text{N}$  data for p38 $\gamma$  - CSH71 (blue round dots) which prefers to bind to the ATP-binding site, whereas  $\beta$ -OG only binds to the lipid-binding site (green triangles). The shifted residues V33, G39, V41, A40, and K69 (indicated by round blue dots, CSH71) are located at the ATP-binding site of p38 $\gamma$ ; red square showed the residues that CSH71 binds in the lipid-binding domain significantly shifted are T244 (blue), I276 and E312. (B) NMR CSP the  $^1\text{H}$ - $^{13}\text{C}$  HMQC spectra in the methyl region for p38 $\gamma$  showed HRD motif (151–153) and its adjacent residues (I149, L154, L159, V161, I169, and L170) highly disturbed in CSH71. It is consistent of others' finding of p38 $\alpha$  that pliable HRD folding of Helix L16 and L16 loop occurs upon compound binding of the LBD, which promotes trans-auto phosphorylation *via* dimerization. (C) 2D interaction diagram of CSH71 in the ATP-binding site of p38 $\gamma$ . V41 (Hydrogen bond); D115 (negative charged); and K118 (positive charged). Many hydrophobic are surrounding CSH71: V33, G39, and V41 on one side of the pocket; T114, D115, and K118 on the other side of the same pocket of p38 $\gamma$ . (D) Docking pose summarized NMR CSP 2D data of p38 $\gamma$  with CSH71, which shows how shifted C-terminal residues that in Y326-V348 segment (L16 loop and L16 helix) posit with those of are located in the ATP-binding site. It is worth to note that along with two residues I149 and L174, Y326 of p38 $\gamma$ , a counterpart of the alternative phosphorylation site Y323 of p38 $\alpha$ , in the interlobe region, may greatly shifted, making possible for opening up DEF pocket based on other's studies (R. A. Engh [14] and O. Livnah [20]). (E) 3D structure of N-terminal segments/domain of p38 $\gamma$  that contains residues that greatly shifted by CSH71. It illustrates a unique structure in the N-lobe p38 $\gamma$  which contains an N-terminal C Helix (yellow) that is sandwiched by C-terminal sequences Helix L16 (red) and L16 loop (blue) where Y326 resides, the site for alternative phosphorylation by ZAP70. The conserved His-Arg-Asp ( $\text{H}_{151}\text{R}_{152}\text{D}_{153}$  motif, colored green), also greatly shifted and likely be protruding toward C Helix as binding of CSH71 to p38 $\gamma$ .

between 50 and 500 nm (Fig. 6B). We treated Hut78 cells with a moderate dosage of 250 nM of CSH71, followed by total RNA isolation and microarray analysis, which we compared to untreated cells. The treatment induced the expression of the pro-inflammatory cytokine TNF $\alpha$  in many top pathways (Table 2). It also caused the up-regulation of the olfactory factor pathway and the down-regulation of Toll-like receptor 5 (TLR5) responses to the chemical stimulation of T cells.

A connection between p38 activation, inflammation, and TNF $\alpha$  expression was first established decades ago. p38 activation promotes the expression of pro-inflammatory cytokines such as TNF $\alpha$  [1,45], and the pathway has been implicated in experimental autoimmune encephalomyelitis (EAE), rheumatoid arthritis [46], multiple sclerosis [47], Alzheimer's disease [48], and inflammatory bowel disease [49]. We previously showed that the knockdown of either p38 $\gamma$  or NFATC4 significantly reduces IL-17A mRNA levels in Hut78 cells [24]. To further understand the role of IL-17A in CTCL, we also monitored the expression of the IL-17A receptor IL17RA—a ubiquitous type I transmembrane glycoprotein that plays a pathogenic role in many inflammatory and autoimmune diseases such as rheumatoid arthritis [50,51] and CTCL [52]—and found that it is constitutively expressed in Hut78 cells (Fig. 6C).

Previous research has indicated that p38 controls IL-17 production in a model of EAE by activating the eukaryotic translation initiation factor 4E/MAPK-interacting kinase (eIF-4E/MNK) pathway [53]. Studies on alternative p38 activation in T cells in EAE have concluded that p38 regulates the production of IL-17 at a transcriptional level through the CAMP-responsive element (CRE), which is the binding site

for activation transcriptional factor ATF2 [54]. However, another study concluded that p38 activation in EAE affects Th17 differentiation rather than IL-17 production [55]. Very likely, IL-17RA positions itself for the upcoming abrupt changes in cytokine IL-17 levels in inflammation, autoimmune disorders, and cancer.

Interestingly, confocal fluorescence microscopy of p-Y323 in p38 and its substrates DLGH1 and IL17RA identified alternatively activated p38 on the newly synthesized nuclear envelopes that surround anaphase chromatin (Fig. 6C, red arrow) and within the interphase nucleus (yellow arrow) of Hut78 cells. This is an intriguing observation, because ZAP70 activity at the TCR complex occurs in the plasma membrane of T cells, and the mechanisms by which phosphorylated Y323/326 p38 migrates to, and remains in, the nucleus are unclear. Here, our data support the notion that Hut78, a malignant T-cell line derived from a CTCL patient, is one of the best cell-based systems in which to study alternative p38 activation by ZAP70.

#### Molecular mechanism of biological effects of CSH71 as a two site-binding ligand on p38 $\gamma$ in CTCL cells

Given that many essential TFs in TCR signaling, including NFATs, are substrates of p38 [56], our results demonstrate not only that alternative p38 phosphorylation is activated in Hut78 cells, but also suggest that the role of p38 in the nucleus involves the regulation of NFAT transcriptional activity.

To determine the nature of nuclear p38 $\gamma$  and its actions on NFATs, we extracted cytosolic and nuclear fractions of Hut78 cells treated with 250 nM or 5  $\mu\text{M}$  CSH71 for 24 or 48 h. The molecular weight of phosphorylated p38 $\gamma$  after 48 h treatment with 250 nM of

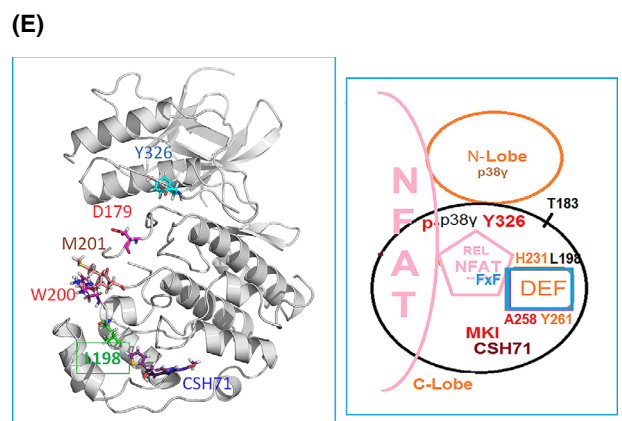
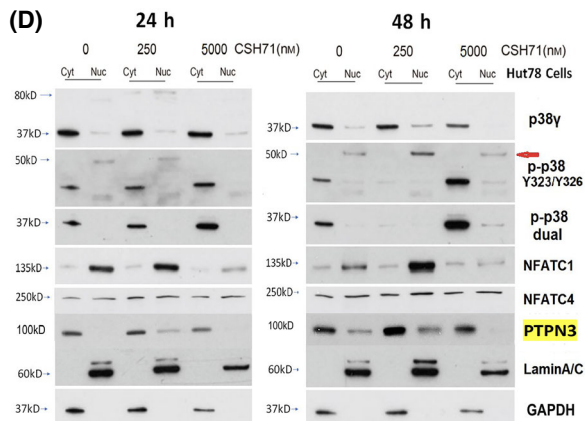
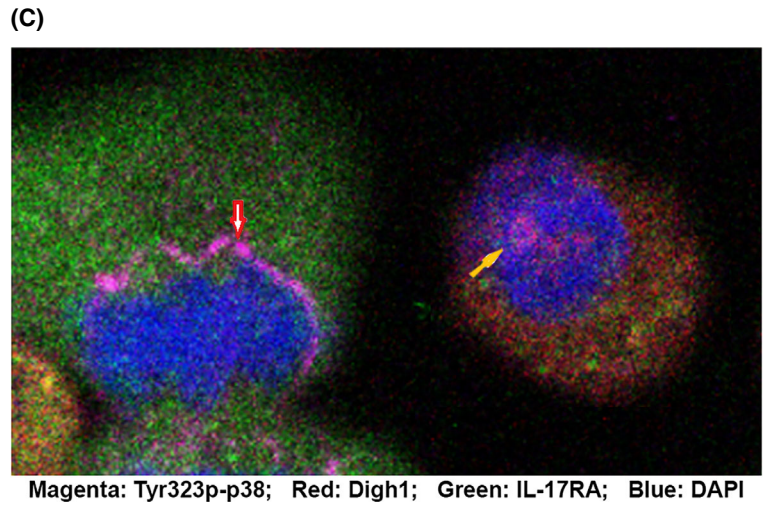
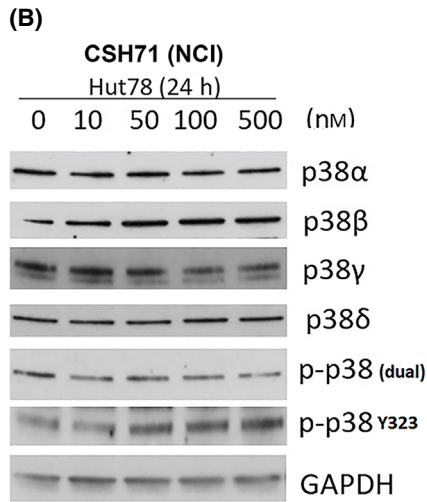
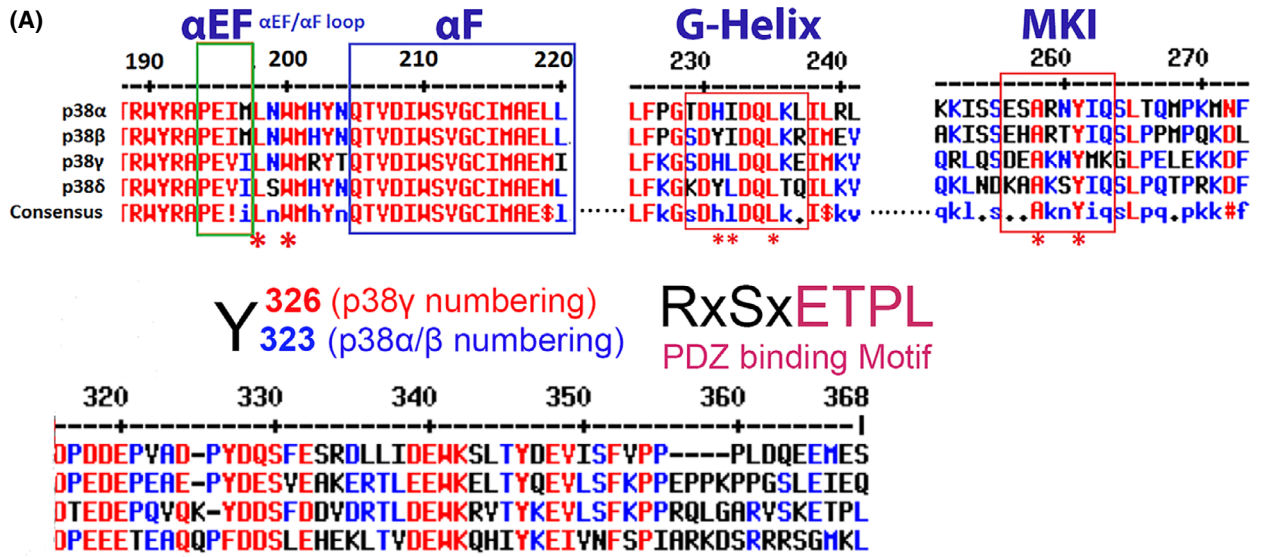


**Fig. 6.** CSH71 inducing alternative p38 and NFAT activation. (A) Illustration of conserved segments of the DEF site interaction pocket (top), including  $\alpha$  EF and  $\alpha$  F loop, G-Helix and MARP insert (MKI) which are structurally conserved among four p38 isoforms, which participates the formation of DEF pocket, many residues are perturbed by CSH71 binding underscored with \*. The segments at bottom are p38s alternative activation site Y<sub>323</sub>/Y<sub>326</sub> by ClustalW2 Consensus alignment diagram analysis with p38 $\gamma$  residue numbering. Residues ETPL is colored pink as PDZ binding Motif that solely existed in p38 $\gamma$ . (B) Western blot analysis to detect protein levels changes upon treatments of CSH71 (NCI) of four isoforms of p38 and two phosphorylated forms dual and alternative p38 together with GAPDH as protein internal loading control. (C) Confocal fluorescence microscopy analysis of untreated Hut78 cells indicates the subcellular location of alternative p38 activation by immunofluorescent staining using the specific antibody Y<sub>323</sub> p-p38. Co-staining with antibodies against DLGH1 (red) and IL17RA (green) was used to identify downstream targets. DAPI was used to stain the nucleus. Alternative p38 activation is seen on the newly synthesized nuclear envelopes that surround anaphase chromatins (red arrow) and also within the nucleus (yellow arrow). (D) Hut 78 cell cytosolic and nuclear fractions lysates treated with indicated doses of CSH71 (250 nM and 5  $\mu$ M) for 24 or 48 h are subject to WB analysis, using anti-p38 $\gamma$ , anti-p-p38 at Y<sub>323</sub> (alternative), anti-p-p38 (dual), anti-PTPN3 and anti-NFATC1, anti NFATC4 antibodies. Anti-Lamin A/C antibody for the Lamin protein as the loading control for nuclear proteins and GAPDH for cytosol proteins. (E) Proposed model of interaction between NFAT with the DEF site of p38 $\gamma$  when the alternative site at Y326 is activated (phosphorylated). Left, 3D p38 $\gamma$  with residues reflect allosteric network from LBD to ATP binding site. Right, NFAT Interaction interact with p38 $\gamma$  via two docking motifs—FxF and LxL sequences; p38 $\gamma$  is also known as ERK6, which implicates similarity with the ERK family; in the REL domain of NFATc4, which contains an Fx motif (F681, F683) at the COOH-terminal that allows interaction with the DEF pocket. Other NFAT members (NFATC1, NFATC2, and NFATC3) have FxY motifs in which possibly allows interaction with ERK. The LxL sequence is specific for other MAP kinases, such as c-Jun NH2-terminal protein kinase (JNK).

CSH71 is approximately 40 kD in the cytosol and 50 kD in the nucleus (red arrow, Fig. 6D, 250 nM, 48 h). This suggests the occurrence of additional post-translational modifications of p-Y326 p38 $\gamma$  in the nucleus of live cells—most likely representing an intermediate/transient form of phosphorylation at pT180 – pY323/Y326.

Surprisingly, neither the dual-phosphorylated form or the alternatively phosphorylated form of p38 are detectable in the cytosol after treatment with 250 nM CSH71 for 48 h, suggesting that certain tyrosine phosphatases are activated in cytosol at low doses of CSH71. (The treatment also causes the disappearance of the dual-phosphorylated form from the nucleus.) We propose that two PDZ domain-containing tyrosine phosphatases reported to be substrates of p38 $\gamma$  [57]—PTPN3 and PTPN4—are responsible. We further speculate that PTPN3 dephosphorylates p-Y323/326 of p38 $\alpha/\gamma$  in the cytosol (Fig. 6D, right). Our western blot analysis confirms these speculations in that 250 nM 48 h treatment increases amounts of tyrosine phosphatases PTPN3 (highlight with yellow), which is reportedly interacts with p38 $\gamma$  via its PDZ-binding motif, may also contribute to the dephosphorylation of Y185 in dually phosphorylated p38 $\gamma$  (disappearance of the band p-p38 in cytosol upon the treatment) that we observed in Fig. 6D (48 h, 250 nM treated). One study has indicated that PTPN3 activation enhances oncogenesis through the dephosphorylation of p38 $\gamma$ , which activates Ras [58]. We hypothesize that PTPN4, which, according to GeneCard, is found mainly in the nucleus, may keep NFATs in a non-phosphorylated, transcriptionally active form in Hut 78 cells.

NFATC1/C4 are nuclear proteins with essential activity in T cells. Consistent with changes in p38 $\gamma$  expression, nuclear NFATC1 is significantly increased in cells treated with 250 nM CSH71, but its expression drastically decreases at higher (5  $\mu$ M) dosages. Interestingly, we observed that the phosphorylated form of NFATC4 (MW = 250 kD) is equally expressed in both cytosol and nucleus of Hut78 cells at both the 24 h and 48 h time points (Fig. 6D). In cells treated with 5  $\mu$ M CSH71, both dual- and alternative phosphorylation is dramatically increased in the cytosol lysates. This suggests that at this higher dosage CSH71 occupies both the ATP-binding site and the LBD of p38 $\gamma$ , resulting in allosteric conformation changes that lead to stress-related p38 activation, drastic reduction of NFAT affinity, and reduced nuclear translocation, subsequently lowering transcriptional activity and eventually causing cell death.

## Discussion

The Engh group [17] has proposed a model of transient dimerization to explain the molecular mechanism of auto-monophosphorylation at T180 (also known as alternative p38 phosphorylation) triggered by Y323 phosphorylation by ZAP70. In this model, the phosphorylation of Y323 in one p38 monomer causes a structural disruption at the L16 loop region, bringing it near T180 of another monomer and facilitating auto-monophosphorylation. A rigid His–Arg–Asp (HRD) motif (H151–D153 in p38 $\gamma$ ) blocks this auto-monophosphorylation when Y323 is unphosphorylated [17].



**Table 2.** Pathway analysis of DE Genes CSH71(NCI) 250 nM vs. Control.

Pathway	Source	P-value	q-value	Top Hits_overlap
Upregulated				
<b>Olfactory transduction</b> - Homo sapiens (human)	KEGG	<b>8.47E-10</b>	2.05E-07	<b>OR5B21; OR52N1; OR52J3; OR56A3; OR4N5; OR1S1; OR11H1; OR2L2; OR10K2; OR6N1; OR8K3; OR2B3; OR6Y1; OR5W2; OR2L8; OR5A1</b>
HTLV-I infection - Homo sapiens (human)	KEGG	0.00072468	0.01288891	JUN; EGR1; ADCY8; ZFP36; <b>TNF</b> ; CREM; ATF3
<b>MAPK signaling pathway</b> - Homo sapiens (human)	KEGG	0.00353542	0.03619249	GADD45A; JUN; <b>TNF</b> ; DUSP5; DUSP4; FLNC
<b>TNF signaling pathway</b> - Homo sapiens (human)	KEGG	0.00376954	0.03619249	PTGS2; JAG1; JUN; <b>TNF</b>
Inflammatory bowel disease (IBD) - Homo sapiens (human)	KEGG	0.00631366	0.05071297	STAT4; <b>TNF</b> ; JUN
Osteoclast differentiation - Homo sapiens (human)	KEGG	0.00698855	0.0527318	CALCR; <b>TNF</b> ; JUN; FOSL2
Leishmaniasis - Homo sapiens (human)	KEGG	0.00837645	0.05637127	PTGS2; <b>TNF</b> ; JUN
Downregulated				
Pathway	source	p-value	q-value	Top Hits_overlap
Pathogenic Escherichia coli infection - Homo sapiens (human)	KEGG	<b>3.10E-05</b>	0.00018592	TUBA3E; TUBA3D; <b>TLR5</b>
Gap junction - Homo sapiens (human)	KEGG	0.00460401	0.01381204	TUBA3E; TUBA3D

Microarray RNA analysis and pathway analysis of Hut78 CTCL cells with 100 nM CSH71 at 48 h treatment. Several significantly up-regulated pathways are in bold, such as the Olfactory transduction pathway, MAPK signaling pathway and TNF pathway. Likewise, down-regulated pathway, Pathogenic Escherichia coli infection, etc. Two representative signaling molecules TNF and TLR5 are highlighted in bold. p-values for two most significantly pathways are Olfactory transduction (unregulated,  $P = 8.47E-10$ , bold) and (down-regulated, Pathogenic Escherichia coli infection,  $P = 3.10E-05$ , bold), respectively.

The HRD motif is conserved throughout all protein kinase families [18]. It supports the configuration of the activation segment [59], and its deformation prevents the auto-monophosphorylation triggered by the phosphorylation of Y323 by ZAP70 [17]. When Y323 is mutated to T323, which bears conformational resemblance to p-Y323, the C-alpha atoms of the TGY motifs are shifted by more than 17A°, promoting conformational changes in the active loop and changing inter-lobe orientation to create a DEF site interaction pocket for substrates such as the TFs ATF2 and ELK1 [16]. (Note that in p38 $\gamma$  the alternative phosphorylation site is Y326.) In this study, we cannot tell upon which isoform of p38 the alternative phosphorylation has taken place, and however, our NMR, IP, and western blot results in Hut 78 cells strongly suggest that it occurs on p38 $\gamma$  (Figs 4C, 5A, D and 6D).

Along with identifying conservative segments defining the DEF site interaction pocket among p38 isoforms (Fig. 6A), our NMR CSP results pinpointed several residues—H231, G243, T244, A258, M262, K263, G264, and L265—in the region that are

significantly shifted by CSH71 (Fig. 5A,B and 2D). We predict that the DEF interaction pocket opens due to shifted p-Y326 in p38 $\gamma$ . The subsequent auto-monophosphorylation at T180, followed by a shift of the entire inter-lobe, would in theory further promote the accommodation of TFs such as ATF2 or NFATs [29]. The 50 kD band of p-Y323 observed in our western blots (Fig. 6D) suggests an intermediate stage of auto-monophosphorylation on T180/T183 that coexists with phosphorylation at Y323/Y326.

p38 $\gamma$  is also known as ERK6, and it shares similarities with the ERK protein kinase family. NFATC4 contains an FxF motif (F681, F683) at the COOH-terminal end of the NFATC4 REL domain that allows interaction with the DEF pocket [3]. A similar motif is also found in other NFAT members (FxF motifs in NFATC1, NFATC2, and NFATC3), which possibly allows interaction with ERK. Two docking motifs—FxF and LxL—appear to facilitate interaction with ERK *via* its DEF site. The LxL sequence is specific for other MAP kinases, such as c-Jun NH2-terminal protein kinase (JNK) [60].

In Fig. 6D, we showed that NFATC1 is increasingly expressed in the nucleus of Hut78 cells in the presence of 250nM CSH71, which correlates with alternative p38 activation (p-Y323) in the nucleus. This implies that NFATs interact with phosphorylated p38 *via* the DEF pocket and activate the TCR signaling pathway after their translocation into the nucleus. Coupled with our data in Fig. 5B,D, we now have novel insight as to how the DEF pocket of p38 opens when alternatively activated to allow NFAT docking, which leads to its entry into the nucleus and the transcription of downstream target mRNA upon CSH71 treatment at low dose (250nM).

CSH71 binds weakly to the ATP-pocket of p38 $\gamma$ , based on its docking pose score ( $-6.82 \text{ kcal}\cdot\text{mol}^{-1}$ ), which is much lower than that of F7

( $-9.81 \text{ kcal}\cdot\text{mol}^{-1}$ , an ATP-pocket binder) [6]. The STD value of CSH71 further supports this notion (Fig. S4B). Therefore, we conclude that CSH71 preferentially binds the LBD of p38 $\gamma$  in Hut78 cells, as it would be displaced from the ATP-binding site by the abundant presence of ATP in live cells. This binding promotes Y326 phosphorylation, which results in opening of the DEF pocket as described. The folding of the pliable HRD motif with the L16 loop and Helix L16 occurs upon CSH71 binding to p38 $\gamma$  (Fig. 5B, pink bracket of shifted residues; Fig. 5E, HRD in green loop), which leading to auto-monophosphorylation of T183. The increased levels of NFATC1 we observed upon CSH71 treatment (250 nM, Figs 6D and 7), further confirms other reports indicating that alternative p38 activation

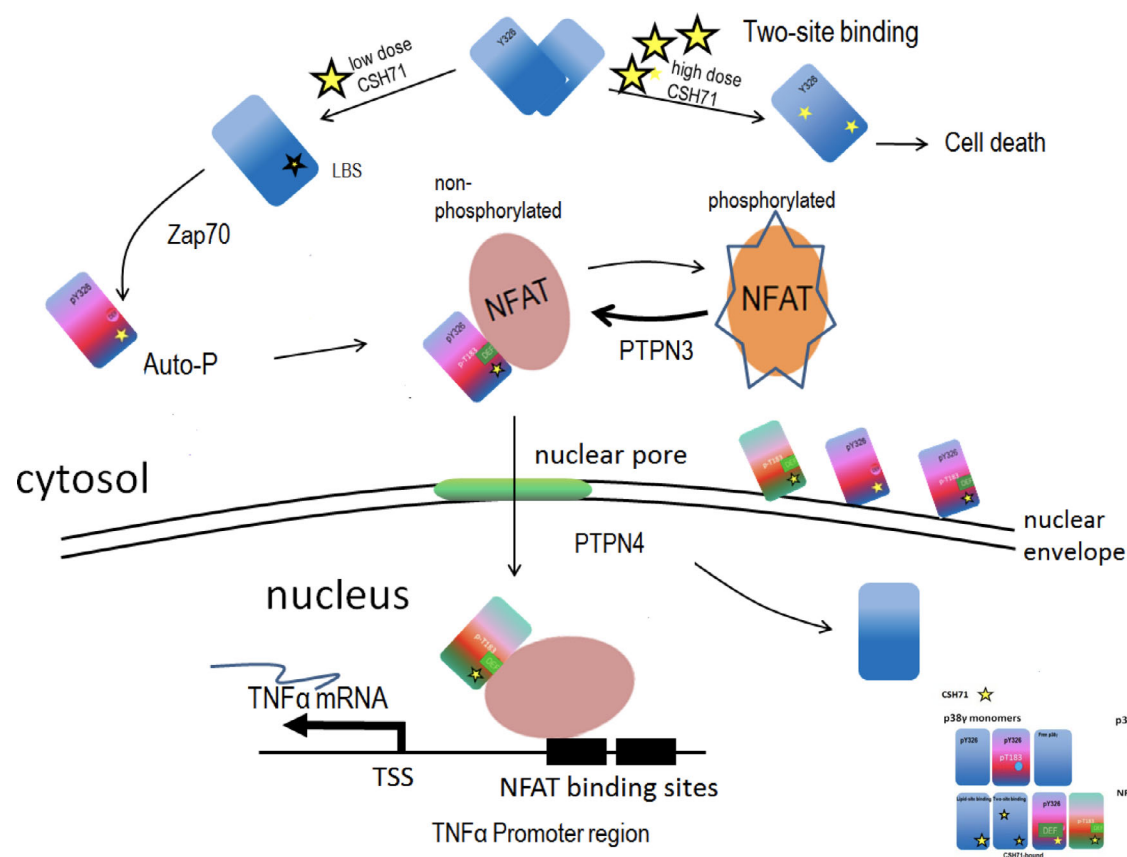


**Fig. 7.** CSH71 as a LBD binder and its biological functionality in CTCL cells. Proposed schematic molecular mechanism by which CSH71 (250 nM) induces TNF $\alpha$ , first to increase cytosolic Y326 phosphorylation of p38 $\gamma$  at the TCR complex proximal to the plasma membrane of T cells and then migrate into the nucleus. Alternative p38 phosphorylation is activated in CTCL cells upon lipid binding, which extends conformational changes to the active loop of p38, followed by interlobe orientation changes, evidenced at Y326 and regions surrounding DEF pocket perturbation, which suggest formation of a DEF site interaction pocket and its availability to other substrates/factors, such as NFATs. Nuclear NFATs then subsequently transcriptionally activate TNF $\alpha$  mRNA in CTCL cells, evidenced by RNA sequencing and pathway analysis at CSH71 treatment (250 nM). At a higher dosage, it is very likely that CSH71 binds to two sites (ATP binding and LBS binding) of p38 $\gamma$  and prevents its dimerization, which further blocks the interaction of p38 $\gamma$  and NFAT thereby preventing its subsequent translocation into the nucleus and thereby cell death.

induces NFATC1 mRNA expression [2]. It is also consistent with previous studies that concluded that alternative p38 activation directs T cells toward the NFAT pathway *via* DLGH1 rather than the NF- $\kappa$ B pathway [44]. Our data suggest a novel pathway in which, at low concentrations (250 nM), CSH71 binds to the LBD of p38 $\gamma$  (not the ATP-binding site) and activates alternative p38 phosphorylation, resulting in the opening of the DEF pocket to accommodate its substrates based on molecular mechanisms proposed by the Engh [15] and Livnah [14] groups.

To further delineate the downstream signaling induced by CSH71 in Hut78 cells, we performed DE analysis after microarray RNA analysis. The pathway analysis (mRNA) of Hut78 cells treated with 100 nM CSH71 for 30 h are listed in Table 2. Our model best explains the increase in TNF $\alpha$ , a critical mediator of immune and inflammatory responses, observed in microarray analysis after CSH71 treatment because there are several NFAT-binding sites in the promoter region of TNF $\alpha$  [28]. We posit that, at a low dose, CSH71 binding to p38 $\gamma$  causes opening of the DEF pocket to accommodate more transcription factor substrates, as indicated by increasing levels of NFAT in the nucleus, and this activates TNF $\alpha$  mRNA expression. In addition, we hypothesize that at this lower concentration, CSH71 activates tyrosine phosphatases PTPN3, as evidenced by the increased amount of PTPN3 in cytosol and the disappearance of the p-Y323 band in western blots of the cytosol and nuclear fractions from treated cells (Fig. 6D, 48 h, 250 nM WB results). We predict that these phosphatases are PTPN3 (we confirmed in cytosol by WB) and PTPN4 (nucleus), which become active 48 h after the initial activation of alternative p38 phosphorylation (Fig. 6D, 24 h). Both tyrosine phosphatases have PDZ domains [61–64], and, interestingly, both are substrates of p38 $\gamma$ , perhaps facilitated by binding *via* the PDZ-binding motif [57,58].

Taken together, Fig. 7 summarizes our experimental data as a molecular model of the proposed mechanism by which CSH71 promotes cytotoxicity in CTCL cells only at high doses. When present at low doses, CSH71 preferentially binds the LBD of p38 $\gamma$ , promoting Y326 phosphorylation and the resulting conformational changes in the DEF pocket to accommodate substrates such as TFs and/or co-factors for transcriptional machinery. This complex subsequently enters the nucleus and activates the expression of TNF $\alpha$ , which promotes pro-apoptotic activity in CTCL cells. In contrast, when present at high levels (5  $\mu$ M), CSH71 occupies both the ATP-binding site and the LBD. This causes phosphorylation of Y326 and a decrease in

tyrosine phosphatase levels that leads to an overall increase in the inactive, phosphorylated form of NFAT in the cytosol. The dramatic reduction of NFAT levels in the nucleus causes cell death.

In summary, we have confirmed the presence of an LBD in p38 $\gamma$  and identified a molecule, CSH71, that binds to both the LBD and the ATP-binding pocket. For the first time, we describe the biological impact of molecules that bind to two sites in p38 $\gamma$ , and we present a model to explain how targeting the LBD with novel drugs could selectively kill CTCL cells.

## Acknowledgements

Research reported in this publication included work performed in City of Hope Cores (Integrative Genomics and Bioinformatics Core, Drug Discovery & Structural Biology Core, and Mass Spectrometry and Proteomics Core) supported by the National Cancer Institute of the National Institutes of Health under award number P30CA033572 and the Light Microscopy Core at City of Hope. Other support included 1R01CA233922-01 (ROSEN) and LLS Grant ID: 6576-19 (ROSEN). The content is solely the responsibility of the authors and does not necessarily represent the official views of the National Institutes of Health.

## Conflict of interest

There are no conflicts to declare.

## Data accessibility

The data that support the findings of this study are openly available in NCBI's Gene Expression Omnibus and are accessible through <https://www.ncbi.nlm.nih.gov/geo/query/acc.cgi?acc=GSE182484>, GEO Series accession number GSE182484.

## Author contributions

XHZ contributed to conceptualization, design and investigation, writing—original draft, and writing—review, editing and corresponding, initializing several key experiments such as screened CSH71 and CSH18, designing CSH18CN, and contributed to immunofluorescence staining and confocal microscopy experiments; CHC contributed to NMR CSP 2D experiments and data analysis and manuscript revisions; HL contributed to conceptualization of docking/virtual screening and generating compound list; JH contributed to cell viability assays, IP and WB experiments; XW contributed to microarray analysis; WH

and JS contributed to NMR 1D and STD experiments and data analysis; DH contributed to compound purification; SN contributed to kinase activity assays; STR contributed to overseeing the lab.

## References

- Zarubin T and Han J (2005) Activation and signaling of the p38 MAP kinase pathway. *Cell Res* **15**, 11–18.
- Alam MS, Gaida MM, Ogawa Y, Kolios AG, Lasitschka F and Ashwell JD (2014) Counter-regulation of T cell effector function by differentially activated p38. *J Exp Med* **211**, 1257–1270.
- Yang TT, Xiong Q, Enslin H, Davis RJ and Chow CW (2002) Phosphorylation of NFATc4 by p38 mitogen-activated protein kinases. *Mol Cell Biol* **22**, 3892–3904.
- Salvador JM, Mittelstadt PR, Guszczynski T, Copeland TD, Yamaguchi H, Appella E, Fornace AJ Jr and Ashwell JD (2005) Alternative p38 activation pathway mediated by T cell receptor-proximal tyrosine kinases. *Nat Immunol* **6**, 390–395.
- Jun JE, Kulhanek KR, Chen H, Chakraborty A and Roose JP (2019) Alternative ZAP70-p38 signals prime a classical p38 pathway through LAT and SOS to support regulatory T cell differentiation. *Sci Signal* **12**, eaao0736.
- Zhang XH, Nam S, Wu J, Chen CH, Liu X, Li H, McKeithan T, Gong Q, Chan WC, Yin HH *et al.* (2018) Multi-kinase inhibitor with anti-p38 $\gamma$  activity in cutaneous T-cell lymphoma. *J Invest Dermatol* **138**, 2377–2387.
- Yin N, Qi X, Tsai S, Lu Y, Basir Z, Oshima K, Thomas JP, Myers CR, Stoner G and Chen G (2016) p38 $\gamma$  MAPK is required for inflammation-associated colon tumorigenesis. *Oncogene* **35**, 1039–1048.
- Browne AJ, Gobel A, Thiele S, Hofbauer LC, Rauner M and Rachner TD (2016) p38 MAPK regulates the Wnt inhibitor Dickkopf-1 in osteotropic prostate cancer cells. *Cell Death Dis* **7**, e2119.
- Zheng S, Yang C, Liu T, Liu Q, Dai F, Sheyhidin I and Lu X (2016) Clinicopathological significance of p38 $\beta$ , p38 $\gamma$ , and p38 $\delta$  and its biological roles in esophageal squamous cell carcinoma. *Tumour Biol* **37**, 7255–7266.
- Qi X, Yin N, Ma S, Lepp A, Tang J, Jing W, Johnson B, Dwinell MB, Chitambar CR and Chen G (2015) p38 $\gamma$  MAPK is a therapeutic target for triple-negative breast cancer by stimulation of cancer stem-like cell expansion. *Stem Cells* **33**, 2738–2747.
- Tomas-Loba A, Manieri E, Gonzalez-Teran B, Mora A, Leiva-Vega L, Santamans AM, Romero-Becerra R, Rodriguez E, Pintor-Chocano A, Feixas F *et al.* (2019) p38 $\gamma$  is essential for cell cycle progression and liver tumorigenesis. *Nature* **568**, 557–560.
- Diskin R, Engelberg D and Livnah O (2008) A novel lipid binding site formed by the MAP kinase insert in p38 $\alpha$ . *J Mol Biol* **375**, 70–79.
- Perry JJ, Harris RM, Moiani D, Olson AJ and Tainer JA (2009) p38 $\alpha$  MAP kinase C-terminal domain binding pocket characterized by crystallographic and computational analyses. *J Mol Biol* **391**, 1–11.
- Comess KM, Sun C, Abad-Zapatero C, Goedken ER, Gum RJ, Borhani DW, Argiriadi M, Groebe DR, Jia Y, Clampit JE *et al.* (2011) Discovery and characterization of non-ATP site inhibitors of the mitogen activated protein (MAP) kinases. *ACS Chem Biol* **6**, 234–244.
- Diskin R, Lebendiker M, Engelberg D and Livnah O (2007) Structures of p38 $\alpha$  active mutants reveal conformational changes in L16 loop that induce autophosphorylation and activation. *J Mol Biol* **365**, 66–76.
- Tzarum N, Diskin R, Engelberg D and Livnah O (2011) Active mutants of the TCR-mediated p38 $\alpha$  alternative activation site show changes in the phosphorylation lip and DEF site formation. *J Mol Biol* **405**, 1154–1169.
- Rothweiler U, Aberg E, Johnson KA, Hansen TE, Jorgensen JB and Engh RA (2011) p38 $\alpha$  MAP kinase dimers with swapped activation segments and a novel catalytic loop conformation. *J Mol Biol* **411**, 474–485.
- Kornev AP, Haste NM, Taylor SS and Eyck LF (2006) Surface comparison of active and inactive protein kinases identifies a conserved activation mechanism. *Proc Natl Acad Sci USA* **103**, 17783–17788.
- Beenstock J, Ben-Yehuda S, Melamed D, Admon A, Livnah O, Ahn NG and Engelberg D (2014) The p38 $\beta$  mitogen-activated protein kinase possesses an intrinsic autophosphorylation activity, generated by a short region composed of the alpha-G helix and MAPK insert. *J Biol Chem* **289**, 23546–23556.
- Bell M, Capone R, Pashtan I, Levitzki A and Engelberg D (2001) Isolation of hyperactive mutants of the MAPK p38/Hog1 that are independent of MAPK kinase activation. *J Biol Chem* **276**, 25351–25358.
- Askari N, Diskin R, Avitzour M, Capone R, Livnah O and Engelberg D (2007) Hyperactive variants of p38 $\alpha$  induce, whereas hyperactive variants of p38 $\gamma$  suppress, activating protein 1-mediated transcription. *J Biol Chem* **282**, 91–99.
- Tian L, Kim MS, Li H, Wang J and Yang W (2018) Structure of HIV-1 reverse transcriptase cleaving RNA in an RNA/DNA hybrid. *Proc Natl Acad Sci USA* **115**, 507–512.
- Bauler TJ, Hughes ED, Arimura Y, Mustelin T, Saunders TL and King PD (2007) Normal TCR signal transduction in mice that lack catalytically active PTPN3 protein tyrosine phosphatase. *J Immunol* **178**, 3680–3687.



- 24 Zhang XH, Ngo VN, Sandoval N, Cui Q, Shi Y, Zain JM, Querfeld C, Guo C, Wu X and Rosen ST (2016) Role of p38 $\gamma$  - NFATc4 - IL17A pathway as a potential therapeutic target in cutaneous T cell lymphoma. *Blood* **128**, 2725. <https://doi.org/10.1182/blood.V128.22.2725.2725>
- 25 Zhang HX, Yin Z, Zhang A, Pillai R, Armstrong R and Rosen ST (2020) DNMT1 and p38 $\gamma$  are inversely expressed in reactive non-metastatic lymph nodes burdened with colorectal adenocarcinoma. *eJHaem* **1**, 300–303.
- 26 Cheung CY and Ko BC (2013) NFAT5 in cellular adaptation to hypertonic stress - regulations and functional significance. *J Mol Signal* **8**, 5.
- 27 Serfling E, Berberich-Siebelt F, Avots A, Chuvpilo S, Klein-Hessling S, Jha MK, Kondo E, Pagel P, Schulze-Luehrmann J and Palmethofer A (2004) NFAT and NF-kappaB factors-the distant relatives. *Int J Biochem Cell Biol* **36**, 1166–1170.
- 28 Falvo JV, Tsytsykova AV and Goldfeld AE (2010) Transcriptional control of the TNF gene. *Curr Dir Autoimmun* **11**, 27–60.
- 29 Yang TT, Xiong Q, Graef IA, Crabtree GR and Chow CW (2005) Recruitment of the extracellular signal-regulated kinase/ribosomal S6 kinase signaling pathway to the NFATc4 transcription activation complex. *Mol Cell Biol* **25**, 907–920.
- 30 Liu W, Zhou M, Li Z, Li H, Polaczek P, Dai H, Wu Q, Liu C, Karanja KK, Popuri V *et al.* (2016) A selective small molecule DNA2 inhibitor for sensitization of human cancer cells to chemotherapy. *EBioMedicine* **6**, 73–86.
- 31 Lipinski CA (2004) Lead- and drug-like compounds: the rule-of-five revolution. *Drug Discov Today Technol* **1**, 337–341.
- 32 Baell JB and Holloway GA (2010) New substructure filters for removal of pan assay interference compounds (PAINS) from screening libraries and for their exclusion in bioassays. *J Med Chem* **53**, 2719–2740.
- 33 Huth JR, Mendoza R, Olejniczak ET, Johnson RW, Cothron DA, Liu Y, Lerner CG, Chen J and Hajduk PJ (2005) ALARM NMR: a rapid and robust experimental method to detect reactive false positives in biochemical screens. *J Am Chem Soc* **127**, 217–224.
- 34 Zhang XH, Zhao C, Seleznev K, Song K, Manfredi JJ and Ma ZA (2006) Disruption of G1-phase phospholipid turnover by inhibition of Ca<sup>2+</sup>-independent phospholipase A2 induces a p53-dependent cell-cycle arrest in G1 phase. *J Cell Sci* **119**, 1005–1015.
- 35 Bührmann M, Hardick J, Weisner J, Quambusch L and Rauh D (2017) Covalent lipid pocket ligands targeting p38alpha MAPK mutants. *Angew Chem Int Ed Engl* **56**, 13232–13236.
- 36 Bührmann M, Wiedemann BM, Müller MP, Hardick J, Ecke M and Rauh D (2017) Structure-based design, synthesis and crystallization of 2-arylquinazolines as lipid pocket ligands of p38 $\alpha$  MAPK. *PLoS One* **12**, e0184627.
- 37 Tong L, Pav S, White DM, Rogers S, Crane KM, Cywin CL, Brown ML and Pargellis CA (1997) A highly specific inhibitor of human p38 MAP kinase binds in the ATP pocket. *Nat Struct Biol* **4**, 311–316.
- 38 Getlik M, Simard JR, Termathe M, Grutter C, Rabiller M, van Otterlo WA and Rauh D (2012) Fluorophore labeled kinase detects ligands that bind within the MAPK insert of p38alpha kinase. *PLoS ONE* **7**, e39713.
- 39 Bellon S, Fitzgibbon MJ, Fox T, Hsiao H-M and Wilson KP (1999) The structure of phosphorylated P38 $\gamma$  is monomeric and reveals a conserved activation-loop conformation. *Structure* **7**, 1057–1065.
- 40 Mayer M and Meyer B (2001) Group epitope mapping by saturation transfer difference NMR to identify segments of a ligand in direct contact with a protein receptor. *J Am Chem Soc* **123**, 6108–6117.
- 41 Cala O and Krimm I (2015) Ligand-orientation based fragment selection in STD NMR screening. *J Med Chem* **58**, 8739–8742.
- 42 Shaul YD and Seger R (2007) The MEK/ERK cascade: from signaling specificity to diverse functions. *Biochem Biophys Acta* **1773**, 1213–1226.
- 43 Tanoue T, Maeda R, Adachi M and Nishida E (2001) Identification of a docking groove on ERK and p38 MAP kinases that regulates the specificity of docking interactions. *EMBO J* **20**, 466–479.
- 44 Round JL, Humphries LA, Tomassian T, Mittelstadt P, Zhang M and Miceli MC (2007) Scaffold protein Dlg1 coordinates alternative p38 kinase activation, directing T cell receptor signals toward NFAT but not NF-kappaB transcription factors. *Nat Immunol* **8**, 154–161.
- 45 Feng YJ and Li YY (2011) The role of p38 mitogen-activated protein kinase in the pathogenesis of inflammatory bowel disease. *J Dig Dis* **12**, 327–332.
- 46 Han ZS, Enslin H, Hu X, Meng X, Wu IH, Barrett T, Davis RJ and Ip YT (1998) A conserved p38 mitogen-activated protein kinase pathway regulates Drosophila immunity gene expression. *Mol Cell Biol* **18**, 3527–3539.
- 47 Sweeney SE and Firestein GS (2004) Signal transduction in rheumatoid arthritis. *Curr Opin Rheumatol* **16**, 231–237.
- 48 Kremmentsov DN, Thornton TM, Teuscher C and Rincon M (2013) The emerging role of p38 mitogen-activated protein kinase in multiple sclerosis and its models. *Mol Cell Biol* **33**, 3728–3734.
- 49 Johnson GV and Bailey CD (2003) The p38 MAP kinase signaling pathway in Alzheimer's disease. *Exp Neurol* **183**, 263–268.
- 50 Batalla A, Coto E, Gómez J, Eirís N, González-Fernández D, Gómez-De Castro C, Daudén E, Llamas-Velasco M, Prieto-Perez R, Abad-Santos F *et al.* (2018)

- IL17RA gene variants and anti-TNF response among psoriasis patients. *Pharmacogenomics J* **18**, 76–80. <http://dx.doi.org/10.1038/tj.2016.70>
- 51 Munoz-Aceituno E, Martos-Cabrera L, Ovejero-Benito MC, Reolid A, Abad-Santos F and Dauden E (2020) Pharmacogenetics update on biologic therapy in psoriasis. *Medicina (Kaunas)* **56**, 719.
- 52 Krejsgaard T, Ralfkiaer U, Clasen-Linde E, Eriksen KW, Kopp KL, Bonefeld CM, Geisler C, Dabelsteen S, Wasik MA, Ralfkiaer E *et al.* (2011) Malignant cutaneous T-cell lymphoma cells express IL-17 utilizing the Jak3/Stat3 signaling pathway. *J Invest Dermatol* **131**, 1331–1338.
- 53 Noubade R, Kremontsov DN, Del Rio R, Thornton T, Nagalekar V, Saligrama N, Spitzack A, Spach K, Sabio G, Davis RJ *et al.* (2011) Activation of p38 MAPK in CD4 T cells controls IL-17 production and autoimmune encephalomyelitis. *Blood* **118**, 3290–3300.
- 54 Namiki K, Matsunaga H, Yoshioka K, Tanaka K, Murata K, Ishida J, Sakairi A, Kim J, Tokuhara N, Shibakawa N *et al.* (2012) Mechanism for p38 $\alpha$ -mediated experimental autoimmune encephalomyelitis. *J Biol Chem* **287**, 24228–24238.
- 55 Jirmanova L, Giardino Torchia ML, Sarma ND, Mittelstadt PR and Ashwell JD (2011) Lack of the T cell-specific alternative p38 activation pathway reduces autoimmunity and inflammation. *Blood* **118**, 3280–3289.
- 56 Murphy LO, MacKeigan JP and Blenis J (2004) A network of immediate early gene products propagates subtle differences in mitogen-activated protein kinase signal amplitude and duration. *Mol Cell Biol* **24**, 144–153.
- 57 Chen KE, Lin SY, Wu MJ, Ho MR, Santhanam A, Chou CC, Meng TC and Wang AH (2014) Reciprocal allosteric regulation of p38 $\gamma$  and PTPN3 involves a PDZ domain-modulated complex formation. *Sci Signal* **7**, ra98.
- 58 Hou SW, Zhi HY, Pohl N, Loesch M, Qi XM, Li RS, Basir Z and Chen G (2010) PTPH1 dephosphorylates and cooperates with p38 $\gamma$  MAPK to increase ras oncogenesis through PDZ-mediated interaction. *Can Res* **70**, 2901–2910.
- 59 Krupa A, Preethi G and Srinivasan N (2004) Structural modes of stabilization of permissive phosphorylation sites in protein kinases: distinct strategies in Ser/Thr and Tyr kinases. *J Mol Biol* **339**, 1025–1039.
- 60 Jacobs D, Glossip D, Xing H, Muslin AJ and Kornfeld K (1999) Multiple docking sites on substrate proteins form a modular system that mediates recognition by ERK MAP kinase. *Genes Dev* **13**, 163–175.
- 61 Babault N, Cordier F, Lafage M, Cockburn J, Haouz A, Prehaud C, Rey FA, Delepierre M, Buc H, Lafon M *et al.* (2011) Peptides targeting the PDZ domain of PTPN4 are efficient inducers of glioblastoma cell death. *Structure* **19**, 1518–1524.
- 62 Genera M, Samson D, Raynal B, Haouz A, Baron B, Simenel C, Guerois R, Wolff N and Caillet-Saguy C (2019) Structural and functional characterization of the PDZ domain of the human phosphatase PTPN3 and its interaction with the human papillomavirus E6 oncoprotein. *Sci Rep* **9**, 7438.
- 63 McCoy AJ (2007) Solving structures of protein complexes by molecular replacement with Phaser. *Acta Crystallogr D Biol Crystallogr* **63**, 32–41.
- 64 Prehaud C, Wolff N, Terrien E, Lafage M, Megret F, Babault N, Cordier F, Tan GS, Maitrepierre E, Menager P *et al.* (2010) Attenuation of rabies virulence: takeover by the cytoplasmic domain of its envelope protein. *Sci Signal* **3**, ra5.

## Supporting information

Additional supporting information may be found online in the Supporting Information section at the end of the article.

**Fig S1A–D** NMR spectra and CSP plots indicate residues in LBD of p38 $\gamma$  that have significantly chemically shifted in response to addition of  $\beta$ -OG. The ratio of  $\beta$ -OG to p38 $\gamma$  is 10:1. (E) The titration effects of  $\beta$ -OG to the LBD residues of p38 $\gamma$  by 1H-15N correlation NMR spectra. (A) NMR spectra. Overlay of the  $^1\text{H}$ - $^{15}\text{N}$  HMQC spectra in the amide region for p38 $\gamma$ , free (red) and in complex with  $\beta$ -OG (blue). (B) NMR spectra. Overlay of the  $^1\text{H}$ - $^{13}\text{C}$  HMQC spectra in the methyl region for p38 $\gamma$ , free (red) and in complex with  $\beta$ -OG (blue). (C) CSP plots. The cutoff value in NMR spectra for amide (ppm>0.02) is indicated by red arrows. (D) CSP plots. The cutoff value in NMR spectra for methyl (ppm>0.03) is indicated by red arrows.

**Fig S1E** A zoomed-in view of the partial region in  $^1\text{H}$ - $^{15}\text{N}$  correlation spectra of  $\beta$ -OG with p38 $\gamma$ . Three residues, T244, E297 and M262 in LBD of p38 $\gamma$  are significantly chemically shifted by ligand  $\beta$ -OG.  $\beta$ -OG was titrated into isotope-labeled p38 $\gamma$ . The different color (Red, Yellow, Green, Cyan, Blue) indicated by arrows on each side of three residues refer to a progressive chemically-shift in respond to increasing concentration of  $\beta$ -OG in the presence of p38 $\gamma$  (p38 $\gamma$  :  $\beta$ -OG = 1:0 red, 1:2.5 yellow, 1:5 green, 1:7.5 cyan and 1:10 blue, respectively).

**Fig S2A** Pure CSH71 are isolated from CSH71 (NCI) by HPLC. A. Mass spectrum of CSH71 (Fraction 3 indicated by arrow.) CSH71 (NCI) is from NCI DTP and we showed it contains 3 fractions including nocodazole (Fraction 2), a well-known cell cycle arrest agent that arrests cells at G2/M phase.

**Fig S2B** Purified 3 (pure CSH71) by MASS and is ready for the further experiments such as NMR assays etc.

**Fig S3A** Biological assessments of CSH71 and  $\beta$ -OG. A. Increasing concentrations of CSH71 (pure) were applied to Hut78 CTCL cells for 72 h.

**Fig S3B** Hut78 CTCL cells were treated with indicated concentrations of  $\beta$ -OG for 72h.

**Fig S3C–D** (C) Increasing concentrations of CSH71 (pure) were applied to Hut78 CTCL cells for 72 h. (D) To determine p38 $\gamma$  kinase activity of CSH71 by in vitro kinase activity measured by ADP-glo assays (blue).

**Fig S4A** 1D NMR STD spectra p38 in complex with CSH71 indicate CSH71 bound p38 $\gamma$ . STD NMR 1D  $^1\text{H}$  spectra overlay of compound CSH71 aromatic region in the presence of p38 $\gamma$ .

**Fig S4B** 1D NMR aromatic proton chemical shifts by CSH71 and STD values in complex with p38 $\gamma$  in the absence and presence of ATP.

**Fig S4C** The docking pose in ATP-binding site more agrees with NMR STD result as five-ring group is located inside the pocket, while  $-\text{COOCH}_3$  tail is outside (left). In lipid-binding, more flexible binding of CSH71 in the LBD pocket (right).

**Fig S5** (A) NMR 2D CSP with CSH71 spectra indicate CSH71 bound p38 $\gamma$ . A. 2D NMR CSP titration experiment with CSH71 spectra: overlay of the  $^1\text{H}$ - $^{15}\text{N}$  HSQC spectra in the amide region for p38 $\gamma$ , free (red) and in complex with CSH71 (blue). (B) 2D NMR CSP titration experiment  $^1\text{H}$ - $^{13}\text{C}$  HMQC spectra in the methyl region overlay for p38 $\gamma$ , free (red) and in complex  $\beta$ -OG (blue). (C) Cut-off value for Amide CSP is  $>0.02$  ppm for selected shifted residues V33, G39, A40, V41, and Y326. (D) Cut-off value for Methyl CSP is  $>0.02$  ppm for selected shifted residues L58 and I149.